The 2002 NEHRP Professional Fellowship Report

EVALUATION OF TSUNAMI RISK TO SOUTHERN CALIFORNIA COASTAL CITIES

Mark R. Legg,
Jose C. Borrero, and Costas E. Synolakis

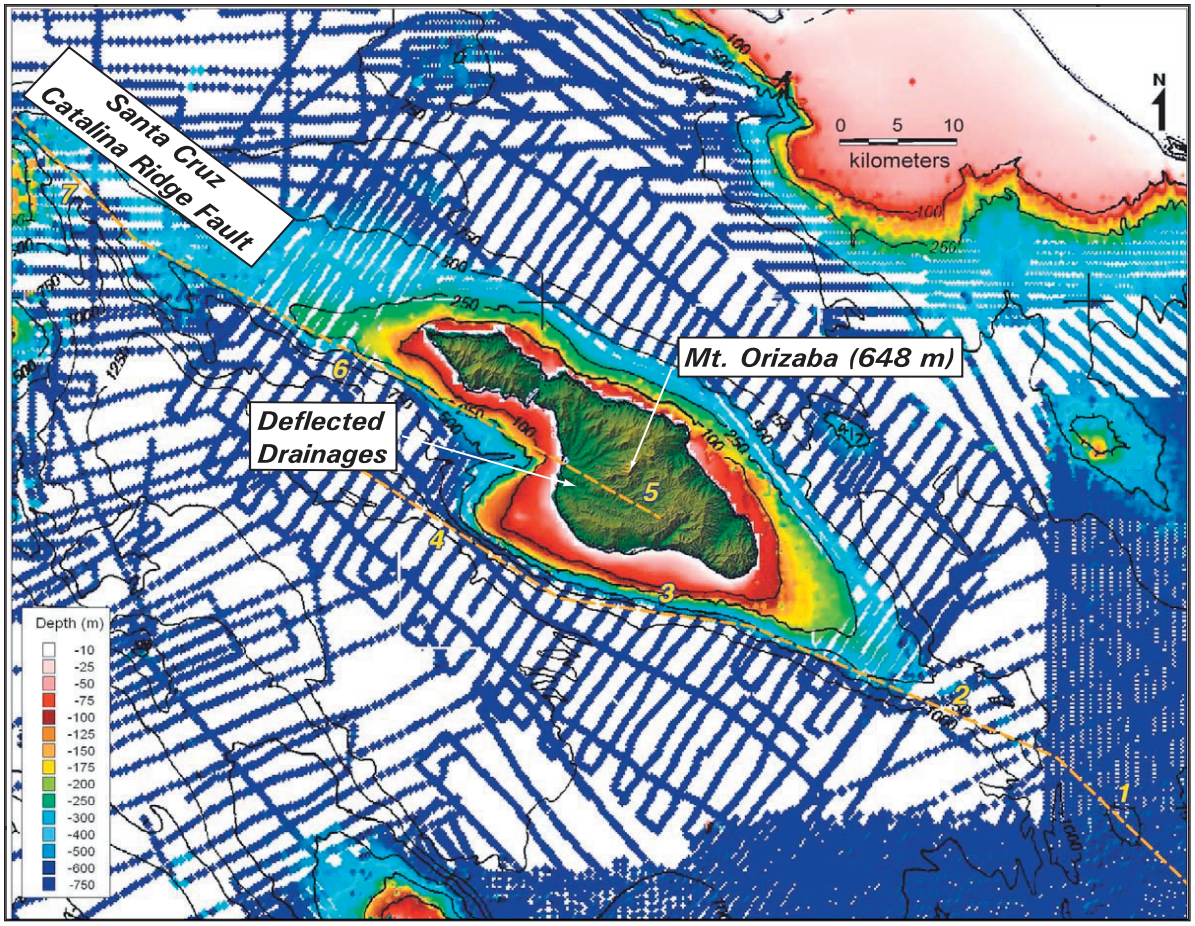

EVALUATION OF TSUNAMI RISK TO SOUTHERN CALIFORNIA COASTAL CITIES

Mark R. Legg,
Jose C. Borrero, and Costas E. Synolakis

January 2003

This research was supported by the 2002 Professional Fellowship,
which was funded by the Federal Emergency Management Agency and administered by the
Earthquake Engineering Research Institute.

PF2002-11

Mark R. Legg, President of Legg Geophysical in Huntington Beach, California, was selected as the 2002 National Earthquake Hazards Reduction (NEHRP) Professional Fellow, awarded by EERI under a cooperative program funded by the Federal Emergency Management Agency (FEMA). Legg's research was conducted in collaboration with Professors Costas E. Synolakis and Jose C. Borrero in the Department of Civil Engineering at the University of Southern California.

Legg has been president of Legg Geophysical since 1992. He has written over 40 technical reports and papers spanning the fields of earthquake engineering, geology and seismology, exploration seismology, natural hazards and risk analysis, and marine geology and geophysics.

Legg earned his B.S. from the Florida Institute of Technology; his M.S. from the Scripps Institute of Oceanography, University of California, San Diego; and his Ph.D. from the University of California at Santa Barbara.

Cover graphic: Santa Catalina Island. The uplift of the island and surrounding seafloor results from the restraining bend (left bend) along the right-lateral San Diego Trough, Catalina Escarpment, and Santa Cruz-Catalina Ridge fault zone. The island platform is located within 50 kilometers of the coastal zone of urban Los Angeles and Orange Counties.

ACKNOWLEDGMENTS

We wish to acknowledge the generous support of the Earthquake Engineering Research Institute for providing the 2002 EERI/FEMA NEHRP Professional Fellowship to Dr. Legg. Susan K. Tubbesing, executive director of EERI, Juliane Lane and Valarie Austin helped to keep the project on track with the monthly progress reports. We also gratefully acknowledge Martin L. Eskijian of the California State Lands Commission, Richard J. McCarthy, executive director of the California Seismic Safety Commission, and Professor Thomas H. Jordan, director of the Southern California Earthquake Center, for their support in applying for the fellowship and ongoing support for offshore earthquake hazard research. Dr. Legg benefited greatly from the SCEC workshop on stress triggering and Dr. Ross Stein's training class for the Coulomb elastic dislocation modeling program. Angie Venturato (NOAA) provided updated bathymetry and topography for use in the MOST modeling program. We truly appreciate working with our talented colleagues at the USC tsunami research center including Vasily Titov (now at NOAA), Matt Swensson (now in Pittsburgh), Diego Arcas, Cristophe Ruschel, Burak Usla, and Ken Rekdahl and Salim Pamukcu who helped us to better understand the tsunami generation and propagation phenomena as well as to assist us in preparing data for completing this project. Lastly, Dr. Legg also benefited greatly from working with the students in his San Diego State University, Department of Geological Sciences class on Compressional Tectonics and Restraining Bends.

TABLE OF CONTENTS

LIST OF TABLES

Page

EVALUATION OF TSUNAMI RISK TO SOUTHERN CALIFORNIA COASTAL CITIES

LIST OF FIGURES

Page

EXECUTIVE SUMMARY

We model the Santa Catalina Island platform as a pop up structure in a major restraining bend along a right-slip fault zone. We are assuming that the shape of the sea floor uplift replicates the finite deformation associated with combined right slip and reverse faulting during major earthquakes on the Catalina fault. We successfully model the seafloor and island uplift with elastic dislocations along two major fault sections comprised of seven individual segments. As observed in several other restraining bends offshore southern California, the two major fault sections are arranged in a right stepping en echelon pattern. These two major fault sections are evident in bathymetry as sea floor scarps and in topography as deflected drainages on the island.

The best fit to the existing bathymetry and topography is achieved with a total fault length of 150 km and segments dipping from 60 to 90 degrees to the northeast. A fault width of 14 km extending from a depth of 0.5 to 1.5 km is used. Fault slips vary from 3.5 to 6.5 m and result in surface uplifts reaching 2.2 m centered on the island near Mt. Orizaba, and subsidence exceeding 1.3 m to the southwest in Catalina Basin. The simulated earthquake has a moment magnitude (M_w) of 7.6 and the predicted surface displacements are comparable to surface faulting measured in recent M_w= 7.0-7.6 earthquakes worldwide.

Tsunami generation as a result of this event effectively creates two wave fronts from the opposite submerged ends of the island platform with initial wave heights of up to 1.5 m. It is important to note that the maximum uplift in this scenario occurs on land and does not directly contribute to tsunami wave height. A third wave front, with smaller amplitude but broad wavelength, is created along the submerged northeast flank of the island platform and rapidly strikes the adjacent Palos Verdes peninsula before the two larger waves strike. Resulting wave interference patterns create zones of elevated run-up along the coast. Coastal run-up of about 1-2 meters was predicted over most of the region from Point Dume to San Onofre for the largest scenario modeled. These run-up values compare well to those observed following the 1927 Lompoc earthquake (1.5-1.8 m). Other recent tsunamis generated by strike-slip earthquakes, such as in the 1994 Mindoro, Philippines, event (M=7.1) that produced maximum run-up reaching 8.5 m, suggest our model predictions may understate the hazard to some extent. Such large run-up may be due to local amplification by this nearshore earthquake; such effects are absent from our offshore model.

Derived from the initial fault model, other scenarios comprised of different segment combinations, slip distributions and earthquake magnitudes are used to evaluate the variability in potential earthquake sources and resulting tsunamis. Earthquake scenarios involving rupture of the northern segments of the Catalina fault, northwest of the island, produce higher run-up in the Santa Monica Bay area, whereas

southern fault segment ruptures produce higher tsunami run-up in the San Pedro Bay area. All scenarios tend to produce higher run-up around the corners of the Palos Verdes peninsula due to its proximity to the source region and wave refraction effects. Plots of tsunami run-up normalized to the maximum uplift predicted in the earthquake source model show areas where tsunami propagation effects, like wave refraction and constructive interference, tend to amplify the wave height. The major areas of tsunami amplification occur along Santa Monica Bay coastline from Marina del Rey to Redondo Beach, and around the San Pedro Bay coast from the Los Angeles and Long Beach harbors to Newport Beach. The largest amplification occurs at Anaheim Bay near Seal Beach. Animations of the wave propagation show that wave refraction due to the Shelf Projection Anticlinorium, between Santa Monica and Redondo submarine canyons in Santa Monica Bay, and Palos Verdes Anticlinorium between San Pedro and San Gabriel submarine canyons focus the tsunami energy at these coastal locations. Another area of amplification occurs near Newport Beach due to wave refraction where the east-trending San Pedro shelf break intersects the coast. Another focusing factor appears due to a tsunami lens or waveguide effect above bathymetric highs, such as Lasuen Knoll, aligned between Santa Catalina Island and the Orange County coast. Due to the long source length parallel to the adjacent coast of these scenarios, predicted amplification patterns are likely to match those for major tsunamis of distant origin as well. Previous studies (Houston, 1980; McCulloch, 1985) show run-up amplitude peaks around Marina del Rey and the Los Angeles/Long Beach harbor areas.

Tsunami potential for the southern California coast near Los Angeles is estimated based on the likelihood of large offshore earthquakes with significant seafloor uplift such as those modeled in this study. In general, the maximum run-up scales with the maximum seafloor uplift produced by the earthquake source, and the amplification patterns result from wave propagation effects. Because accurate slip rates on the major offshore faults are yet undetermined, preliminary estimates of tsunamigenic earthquake occurrence rates are based on a crude comparison of the modeled seafloor uplift per event (from 1-3 m peak-to-trough) divided by the observed total uplift of the Santa Catalina Island platform (about 2,200 m total structural relief) multiplied by the time since the uplift began. Assuming the restraining bend pop-up structure of Santa Catalina Island formed in Plio-Pleistocene time, i.e., during the past 3 Myrs, large tsunamigenic earthquakes would have recurrence intervals of 2,000-5,000 years. Considering the additional active faults in the southern California offshore area, and an overall offshore rate of right-slip estimated at 5-10 mm/yr, large offshore tsunamigenic earthquakes may have recurrence times of 200-500 years. Large offshore earthquakes may directly generate tsunami through tectonic seafloor uplift or indirectly by triggering large submarine slope failures. Although locally generated tsunamis in the southern California coastal region are unlikely events, their return periods

appear similar to those of large earthquakes (M_w>7) on many other low slip-rate faults of the region where recent events have occurred. The tremendous value of coastal property, including major port facilities, urban infrastructure and large populations, creates the potential for great loss from these infrequent offshore events. Clearly, more careful analysis of offshore faulting and rates of earthquake activity are needed to provide more accurate estimates of this risk.

EVALUATION OF TSUNAMI RISK TO SOUTHERN CALIFORNIA COASTAL CITIES

INTRODUCTION

Locally-generated tsunamis from major active faults offshore southern California threaten the nearby coastal cities. Disruption of operations at important port facilities due to tsunami attack could severely impact regional and nationwide economies. Historically, potential for tsunami generation from local sources has been considered insignificant because most of the faulting in the southern California region is strike-slip in character (Fig. 1). Yet, major thrust and reverse faulting occurs throughout the western Transverse Ranges (WTR) including historical tsunami occurrence following strong earthquakes in the Santa Barbara Channel region and west of Point Conception (Table 1; McCulloch, 1985; Lander et al, 1993; McCarthy et al, 1993). Furthermore, the major strike-slip faults offshore southern California, south of the WTR, have sinuous traces with many bends and step-overs. Local tectonic convergence at restraining bends and step-overs creates folding and seafloor uplift whereas local tectonic divergence at releasing bends and step-overs produces extension and seafloor subsidence (Legg and Kennedy, 1991).

Table 1. Possible Locally-Generated Tsunami Along the Southern California Coast

Event	Year	Magnitude	Area Affected	Waves Reported
1	1812	7-7½ (M_I)	North Shore, Santa Barbara Channel	3- to 4-m run-up at Gaviota
2	1855	6 (M_I)	San Juan Capistrano	Two unusually heavy sea waves
3	1862	5½-6 (M_I)	San Diego Bay	< 1-m
4	1879	?	Santa Monica Bay	Affected Santa Monica
5	1927	7.3 (M_S)	Point Arguello	1.8-m run-up at Surf, 1.5-m run-up at Port San Luis
6	1930	5.25 (M_W)	Santa Monica Bay	Local oscillations to about 0.6 m
7	1933	6.25 (M_W)	Long Beach	Uncertain records
8	1979	5.0 (M_L)	Santa Monica Bay	Local oscillations (?)
9	1989	5.0 (M_L)	Santa Monica Bay	Local oscillations (?)

Modified and updated from McCulloch (1985), McCarthy et al, (1993)
Magnitude Scale: M_W = Moment Magnitude; M_S = Surface Wave Magnitude; M_L = Local (Richter) Magnitude; M_I – Seismic Intensity Magnitude; ? = Magnitude Not Given or Unknown

Rapid seafloor deformation at these fault bends and offsets may generate local tsunamis that could be damaging to nearby coastal areas. This project examines a large seafloor uplift, the Santa Catalina Island platform (Fig. 2), and its potential for generating destructive local tsunami that attack the southern California coastal area near metropolitan Los Angeles.

Southern California Offshore Faulting and Tectonic Evolution

The submarine area west of southern California is called the California Continental Borderland (Shepard and Emery, 1941). The physiography of the Borderland consists of generally northwest-trending ridges, banks, and basins, considered to represent a submerged equivalent of the Peninsular

Ranges (Moore, 1969). More recent studies, however, show that Borderland geologic structure and physiography is rather similar to the Basin-and-Range province (Legg, 1991). Offshore basins and banks represent tilted fault blocks, horsts, and grabens formed during Middle Miocene oblique extension as the Pacific-North America transform fault plate boundary evolved (Bohannon et al, 1990; Legg, 1991; Crouch and Suppe, 1993; Bohannon and Geist, 1998). This ridge and basin structure persists as the San Andreas fault system accommodates about 52±2 mm/yr of right shear between the Pacific and North America tectonic plates (DeMets and Dixon, 1999). A significant component of the relative motion, perhaps as much as 20% (5-10 mm/yr), occurs on faults west of the southern California coastline (Legg, 1991; Larson, 1993; Bennett et al, 1993). Oblique-slip on curvilinear and offset fault segments locally maintains or enhances the inherited structural relief and may produce tsunamis during large submarine earthquakes.

Major faults offshore southern California with northwest trends are right-slip in character (Vedder et al, 1974; Vedder et al, 1986; Clarke et al, 1987; Legg et al, 1989) like the San Andreas fault. Offshore faults with east-west trends lie generally within or along the edge of the WTR and show thrust, reverse, or left-slip character. Vertical deformation occurring along coastal and offshore fault zones is directly responsible for uplift of coastal and island marine terraces (Lajoie et al, 1992). Uplifted marine terraces are prominent, not only within the WTR where major folding and thrust faulting occurs, but also along the southern California coast where right-slip faulting predominates. Relative uplift or subsidence of the latest Pleistocene shoreline (18 ka) is shown by warping of this regional submerged marine terrace platform (C. Goldfinger, 2000). As shown by Legg and Kennedy (1991), the sinuosity and en echelon character of real strike-slip faults produces local uplifts at restraining bends and pull-apart basins at releasing offsets.

Restraining Bends and Pull-Apart Basins

Local changes in the trend of strike-slip fault zones are known to result in areas of convergence or divergence depending on the change in local fault strike relative to the azimuth of overall transcurrent (strike-parallel) fault movement (Fig. 3; Crowell, 1974; Christie-Blick and Biddle, 1985; Sylvester, 1988). For right-lateral faults common to southern California, a bend or step to the right in the fault trace results in an area of divergence forming a releasing bend or step-over with a sag or pull-apart basin (Fig. 3). If the right-slip fault bends or steps to the left, then an area of convergence occurs with local folding and uplift at the restraining bend. Rapid vertical seafloor deformation during large earthquakes at these fault irregularities may generate a local tsunami. Long term oblique deformation at these irregularities may form deep, sediment-filled pull-apart or sag basins along extensional (transtensional) fault segments

and elevated submarine ridges or islands at major restraining (transpressional) segments.

Numerous features on the seafloor offshore southern California may be attributed to oblique deformation along the major right-slip fault zones of the Inner Borderland (Fig. 4). It appears that for every restraining bend uplift there is a related releasing bend sag or pull-apart basin (Legg et al, 1999). Vertical-axis rotation of crustal blocks in these zones of simple shear further accentuates the fault irregularities. Indeed, the wholesale clockwise rotation of the WTR since the middle Miocene initiation of the Pacific-North America transform fault plate boundary in southern California results from this simple shear (Kamerling and Luyendyk, 1979; Luyendyk, 1991). The resulting zone of north-directed convergence at the southern boundary of the WTR likely enhances the formation of restraining bend and transpressional uplift apparent in the northern Borderland (Fig. 4). Yet, prominent northwest-trending ridges such as the Santa Cruz-Catalina Ridge, and recent earthquakes with thrust fault mechanisms on northwest-trending fault planes (e.g., 1986 Oceanside, Hauksson and Jones, 1988) show that north-south principal shortening as the WTR rotates into northeast-directed shortening farther south and east along coastal and offshore southern California. Large-scale evidence of this northeast-directed convergence may be apparent in the thrust reactivation of the regional Oceanside detachment fault system (Crouch and Suppe, 1993; Rivero et al, 2000). Strain partitioning likely occurs with right-slip accommodated on the vertical or high-angle northwest-trending faults and thrusting or oblique-reverse faulting on the low to moderate dipping faults (Nicholson and Crouch, 1989).

Uplifts at strike-slip fault restraining bends are called “pop-ups” (cf., McClay and Bonora, 2001). Analog modeling of restraining bends and step-overs along strike-slip faults show a general rhomboid-shaped uplift pattern with numerous secondary and branch faults bounding and within the pop-up (Wilcox et al, 1973; McClay and Bonora, 2001). The equivalent subsiding extensional structure at the idealized pull-apart basin is called a “rhombochasm” (Crowell, 1974). Several restraining bend pop-up structures identified within the Inner Borderland show the rhomboid shape (Fig. 4) at scales ranging from a few kilometers wide and several kilometers long (offshore west of Oceanside) to more than 20 kilometers wide by 80 kilometers long (Santa Catalina Island platform). Structural relief on these features ranges from a few hundred meters to more than two kilometers.

Restraining bend pop-ups are known onshore in southern California. For example, Signal Hill along the Newport-Inglewood fault zone in the Los Angeles Basin, Mount Soledad along the Rose Canyon fault in La Jolla (San Diego), and possibly the San Bernardino Mountains along the San Andreas fault or the San Gabriel Mountains along the San Gabriel fault (Fig. 1; Morton and Matti, 1993; Weldon et al, 1993) are pop-ups. The largest restraining bend known in the region is the “big bend” along the southern San Andreas fault, located between the Salton Trough and the California Coast Ranges (Fig. 1).

Transpression along this bend is accommodated by a complex array of geologic structures including smaller pop-ups referred to above as well as oblique-reverse and thrust faulting throughout the Transverse Ranges.

EARTHQUAKE MODELING

Modeling of potential large earthquake sources in the southern California offshore region is necessary to predict the seafloor deformation that may produce a tsunami. As discussed above, the geometric irregularities along active strike-slip faults produce significant seafloor uplift or subsidence recognizable in the seafloor morphology as restraining bend pop-ups and releasing bend sags or pull-apart basins. Increased normal stress upon the transpressional fault surface along a restraining bend would be expected to lock the fault and result in infrequent large earthquakes. Such may be the case for the San Andreas fault, including the section that passes through the Big Bend (Fig. 1) where infrequent large earthquakes have been identified from paleoseismological investigations (Sieh et al. 1989). Relative quiescence in microseismicity occurs during the interseismic period between major plate boundary earthquakes (Hill et al., 1990), with great earthquakes (M_W>7.5) rupturing this fault zone in 1812 and 1857 (Jacoby et al, 1988). Assuming similar behavior for major offshore faults, the transpressional zones where large restraining bends occur may represent the sites of prehistoric and future large earthquakes (M_w>7). Indeed, seventy years of seismicity data for southern California show few earthquakes along the Catalina fault (Fig. 5). With the co-seismic seafloor uplift associated with large offshore restraining bend earthquakes, the potential for destructive local tsunamis in the California Continental Borderland may be realized.

Major restraining bends in the area offshore southern California include (Fig. 4): the Oceanside and Dana Point segments of the offshore Newport-Inglewood (South Coast Offshore) fault zone (Fischer and Mills, 1991); the Palos Verdes Hills, offshore Palos Verdes Anticlinorium, and Lasuen Knoll along the Palos Verdes fault zone (Nardin and Henyey, 1978; Mann and Gordon, 1996); the Santa Catalina Island platform along the San Diego Trough-Catalina fault zone (Junger, 1976; Mann and Gordon, 1996); the southern half of San Clemente Island and the “Bend Region” of the San Clemente fault zone (Legg and Kennedy, 1991; Legg et al, 1999). All of these features show folding and faulting of late Cenozoic, and locally, Holocene sediments as well as seafloor uplift ranging from 10 meters to more than 1 kilometer (cf., Vedder et al, 1974; Vedder et al, 1986; Clarke et al, 1987). In addition, numerous earthquakes have been located along these major fault zones, although epicenters are sparse along the restraining bend segments (Fig. 5). Exceptions occur at the southeast end of San Clemente Island where the December 16, 1951 earthquake (M_L=5.9) and offshore Oceanside where the July 13, 1986 (M_S=5.8) earthquake struck. Both of these earthquakes had unusual aftershock sequences with few events for the 1951 earthquake (Legg, 1980) and a rich sequence for the 1986 earthquake (Hauksson and Jones, 1988). Considering the length of the restraining bend fault segments, about 30-150 km assumed to be locked in

an interseismic period, and the overall length of these major fault zones that exceeds 100-300 km, we recognize numerous potential sources of large offshore earthquakes that may generate local tsunamis.

Santa Catalina Island Restraining Bend

The Santa Catalina Island platform represents the largest restraining bend pop-up recognized in the northern California Continental Borderland (Figs. 4 & 6). Proximity to the coastal zone of urban Los Angeles and Orange Counties (within 50 kilometers), orientation so as to direct tsunami energy towards the southern California coast (coast parallel trend), and size of the seafloor uplift (exceeding 1,300 square kilometers and almost 2,000 meters seafloor relief) suggests that the Santa Catalina Island restraining bend represents the most serious local tsunami threat to coastal southern California. Notwithstanding the closer location of the Palos Verdes fault zone to coastal Los Angeles and Orange counties, the deeper water and greater size of the Santa Catalina Island uplift imply that large earthquakes on the Catalina fault would move larger volumes of sea water for greater distances (larger earthquake displacements) than would large earthquakes along the Palos Verdes fault zone. Consequently, this study focuses upon the earthquake potential, seafloor uplift and tsunami generation from the Santa Catalina Island restraining bend pop-up.

Elastic Dislocation Model

Most studies of earthquake-generated tsunami use elastic dislocation modeling to predict the seafloor displacement based upon an earthquake source model (e.g., Satake and Somerville, 1992; Geist, 1998). Often, these studies find that earthquake source models involving spatially uniform slip over a simple fault rupture surface underestimate the observed tsunami run-up (Geist, 2002). In some cases, other mechanisms, such as submarine landslides, may produce the locally observed higher run-up and inundation levels (e.g., Synolakis et al., 2002). Yet, most earthquake-related tsunamis are caused by tectonic displacements, although large earthquakes may sometimes generate substantial submarine landslides in the epicentral area. As noted by Geist (2002), complex rupture processes have important effects on the tsunami generation and local run-up. Real earthquakes have non-uniform slip distributions on the active fault surface (e.g., Hartzell and Heaton, 1983; Wald and Heaton, 1994), often involve multiple fault segments (e.g., 1992 Landers earthquake, Sieh et al., 1992), and high slip patches tend to be the major tsunami source (Geist, 2002; Peru earthquake, Okal et al, 2001). To address these issues, we develop a multiple segment fault rupture and earthquake source model for tsunami generation. Because source complexities such as variable rigidity along the fault surface and highly irregular slip distributions are difficult to predict with limited subsurface data, our model retains the simplicity of

uniform slip patches and constant rigidity, but uses several patches with different fault geometry and slip vectors. For the tsunami model, the static displacement due to the earthquake, in particular, the vertical displacement is used to model the initial wave heights. Thus, to calibrate this simple model to more realistic earthquake and faulting parameters, we attempt to match the shape of the seafloor uplift observed at the restraining bend (Legg and Borrero, 2001). For this study, the elastic dislocation model is developed to produce a pattern of seafloor uplift that mimics the shape of the Santa Catalina Island uplift (Fig. 6 & 7). The fault displacements used for the earthquake source in the model are scaled to represent realistic displacements observed in other large earthquakes throughout California and the world (e.g., Wald and Heaton, 1994; Wells and Coppersmith, 1994).

The elastic dislocation model used is based on the work of Okada (1985, 1992). The deformation at the sea floor is computed using Okada's (1985) formulas for surface displacement due to shear and tensile faults in a homogeneous, elastic, half space. To test alternative fault rupture models before selecting one for use in the tsunami generation, the Coulomb program (King et al., 1994; Toda et al., 1998) was used to compute vertical displacement at the surface to compare with observed uplift patterns. This program allowed quick computation of numerous candidate source models so that we could more effectively define our final tsunami earthquake source.

The surface trace of faulting used for the earthquake model is based on geological mapping in the Santa Catalina Island region (Vedder et al, 1974; Vedder et al., 1979; Vedder et al, 1986; White, 1991), available seismic reflection profiles including the LARSE deep crustal imaging data (ten Brink et al, 2000). White (1991) identified a major northwest-trending strike-slip fault cutting the southwest side of the island based on interpretation of satellite imagery and field studies. Shaded relief maps of the digital elevation data for Santa Catalina Island show deflected canyons along the trace of this previously unrecognized fault (Fig. 6b). A short segment of this fault, with a 68 degree northeast dip, is exposed in lower Bullrush canyon along the western side of the island (White, 1991). Combining bathymetric soundings from the NOAA hydrographic data (NOS, 1999) plotted as shaded relief images with the digital elevation image provides a graphical display of the morphology of the Santa Catalina Island restraining bend pop-up (Fig. 6).

Preliminary trials with the elastic dislocation modeling showed that a reasonable fit to the mapped faulting and morphology of the uplift could be achieved with seven active fault segments (Table 1). The geographic location, strike, and length of each fault segment were derived from the existing fault maps. The seven fault segments comprise two major fault sections—one along the northwest part of the uplift and the second along the southwest flank of the uplift. These two fault sections form a 90-km long restraining bend with a 7.5-10 km releasing (right) overlapping fault stepover. The total fault length

modeled is about 140 km and the restraining bend segments trend 18-36 degrees obliquely to the west of the larger right-slip fault system as defined by the Santa Cruz-Catalina Ridge and the San Diego Trough fault zones. Uplift of the Santa Cruz-Catalina Ridge fault zone suggests that it is transpressional to some degree although the 1981 Santa Barbara Island earthquake in this area showed nearly vertical strike-slip on an azimuth of 318 degrees (Corbett, 1984). The vertical strike-slip fault segments in our Santa Catalina Island uplift model have slightly more west-trending strikes (Table 2) and we include a small component of reverse-slip to account for uplift on the ends of the island platform.

Table 2. Major Fault Segments for Santa Catalina Uplift Tsunami Models

Segment	Slip (m)	Length (km)	Width (km)	Strike (degrees)	Dip (degrees)	Slip Angle[1] (degrees)	Depth[2] (km)
1	4.0	21.932	14.000	313	89	172.9	0.500
2	5.0	28.231	14.000	293	85	143.1	1.000
3	4.8	16.125	14.850	277	70	123.7	1.000
4	3.6	20.248	14.000	303	80	146.3	1.000
5	6.4	8.062	14.000	300	80	149.0	1.500
6	4.5	40.249	14.000	297	80	153.4	1.000
7	4.1	29.698	14.000	315	89	166.0	0.500

[1]Rake of slip vector measured from down-dip direction, pure right-slip = 180 degrees.

[2]Depth to top of fault plane below ground surface (top of elastic half-space).

Fault dip and down-dip width are poorly constrained for many offshore faults including those along the Catalina Escarpment. Recognizing the overall strike-slip character of the San Diego Trough – Catalina – Santa Cruz Ridge fault zones, the fault dip is expected to be near vertical. The predominately right-slip fault segments (#1 and #7) in our model are assigned vertical dip. Seismic reflection profiles across the fault zone at the northwest and southeast ends of the Santa Catalina Island uplift show vertical or very steep fault dips (Vedder et al, 1974; Vedder et al, 1986; ten Brink et al, 2000). The straight trace of the shallow faulting, from seismic profiles and the seafloor escarpment, attest to the steep fault dip. Where the fault bends toward the west, we inferred that the dip shallows slightly, from 60-80 degrees northeast dip. The shallowest dip lies along the most west-trending segment (#3). The modeled dips of the restraining bend fault segments are consistent with those inferred for the Palos Verdes fault (70 degrees southwest) beneath the Palos Verdes Hills (Ward and Valensise, 1994) and for the Loma Prieta earthquake (Plafker and Galloway, 1989).

Down-dip width and depth to the top of faulting were variables tested by the elastic dislocation modeling. If the fault width is too small with a shallow fault, the predicted uplift pattern is too narrow compared to the observed seafloor/island morphology (Fig. 7a-b). If the top of faulting is set too deep,

then the predicted uplift pattern is too broad and smoothed compared to the observed morphology (Fig. 7d). The best-fitting model uses a down-dip fault width of 14 kilometers and top of faulting varying along strike from 0.5 to 1.5 kilometers (Fig. 7c, Table 1). Thus, we predict that brittle faulting (elastic deformation) occurs to depths of 16 kilometers in the vicinity of the Santa Catalina Island restraining bend. This is somewhat deeper than the typical 8-12 kilometer focal depths of strike-slip earthquakes in California (Sibson, 1982) although depths of 15 kilometers are reported in the San Diego area (Magistrale, 1993). Thrust and reverse faulting earthquakes often initiate at greater depths, sometimes exceeding 20 kilometers in the Transverse Ranges (Lee et al., 1979; Hauksson et al., 1995), and the focal depth of the 1989 Loma Prieta earthquake, along the Santa Cruz Mountains restraining bend section of the San Andreas fault, was nearly 18 kilometers deep (Plafker and Galloway, 1989). Furthermore, the LARSE data at the south end of Santa Catalina Island suggest a sub-vertical fault extending beyond 8-10 kilometers depth (ten Brink et al, 2000). Therefore, we believe that our elastic dislocation model with brittle faulting extending to 16 kilometers depth is reasonable.

The presence of a releasing step-over in a major transpressional fault section, along a restraining bend, appears to be common in the southern California area (Legg et al, 1999). For example, Cajon Pass along the southern San Andreas fault appears to represent such a releasing step-over, where the Banning fault steps to the northeast (to the right) along the Mission Creek and principal traces of the San Andreas fault (Fig. 1; Morton and Matti, 1993). The tectonic geomorphology of Cajon Pass is further complicated by the interaction between the San Jacinto and San Andreas faults, which converge transferring right-slip from the San Jacinto fault zone (Glen Helen fault) to the San Andreas fault along another releasing step-over. This fault pattern and fault interaction appears to be replicated where the San Clemente fault merges with the Catalina fault at the northwest end of the island uplift (Fig. 1).

Although the offshore slip rates are lower than those of the San Andreas and San Jacinto fault systems, the geographical scale of these major fault interactions is remarkably similar. Thus, subsurface fault geometry may also be similar allowing structural images from carefully located seismicity in the more active and heavily instrumented onshore fault system to infer that structure for the Catalina fault. According to Seeber and Armbruster (1995), in the San Gorgonio Pass region, the San Andreas fault appears as a continuous, northwest-trending, steeply northeast-dipping, right-slip fault that extends to depths as great as 23 km. Oblique reverse-slip along a moderately northeast-dipping San Gorgonio Pass thrust fault is inferred to lie in the hanging wall to the northeast of the San Andreas fault. This fault may offset the steeper right-slip fault in the shallow subsurface, accounting for the discontinuous surface trace of the San Andreas fault in this area, but their data are insufficient to resolve this shallow structure. The deep extent of the right-slip San Andreas fault and its steep dip are consistent with our model for the

Catalina fault. Our Catalina fault model includes a moderate north-dipping oblique-reverse fault segment (#3) at the southwest side of the island, it is not inferred to cut across the more steeply dipping segment (#5) that terminates near the southeast end of the island. Thus, unlike the Seeber and Armbruster (1995) interpretation for the San Andreas fault, we model a discontinuous fault beneath the restraining bend uplift. For our ultimate goal of modeling tsunami run-up generated by earthquakes on the Catalina fault, the details of the deep fault structure are less important than matching the shape of the observed Santa Catalina Island uplift.

The last parameters to be set in the elastic dislocation model for the large earthquake on the Santa Catalina Island restraining bend are the displacements on each fault segment. For a total fault rupture length of about 140 kilometers, empirical relations of magnitude versus fault rupture length suggest earthquake magnitudes of about 7.4-7.6 (Wells and Coppersmith, 1994). Recent large strike-slip earthquakes in southern California and Turkey involved surface rupture lengths exceeding 70 kilometers (M_w=7.3) for Landers (Wald and Heaton, 1994) and about 145 kilometers (M_w=7.4) for Izmit, Turkey (Barka et al., 2002). Maximum displacements estimated from modeling the strong ground motion for these earthquakes ranged from about 7 meters for Landers (Wald and Heaton, 1994), and 5.2 meters for Izmit (Barka et al., 2002). Vertical displacements from the 1989 Loma Prieta earthquake (M_w=6.9) were comparable to the lateral displacements, about 1.3 meters (Plafker and Galloway, 1989).

TSUNAMI MODELING

The tsunami modeling process can be divided into three parts: generation, propagation, and run-up (Liu et al., 1991; Titov and González, 1997). The generation phase includes the formation of an initial disturbance on the ocean surface due to a coseismic deformation of the sea floor. In this case, the initial condition for the long wave propagation is obtained directly from the expected coseismic deformaition of the earth's surface. The deformation on the sea floor is modeled using Okada's (1985) formulas for surface deformation as described in the preceding section. The sea floor deformation field modeled by the elastic dislocation model (Fig. 8) is translated directly to the water surface and used as an initial condition for the propagation and run-up phases.

For tsunami propagation and run-up, the model known by the acronym MOST (Method of Splitting Tsunami; Titov and González, 1997) was employed. This model uses the fully non-linear, depth averaged, shallow water wave equations in characteristic form to simulate the propagation of long waves over an arbitrary bathymetry. For run-up, the model uses a moving boundary algorithm (Titov and Synolakis, 1995; Titov and González, 1997).

For this study, a 400-meter bathymetry and topography grid provided by NOAA (Angie Venturato, personal communication) was used over the simulation area (Fig. 9). The MOST code re-grids the data for optimal numerical simulation using an appropriate and constant number of grid points per wavelength, thereby accounting for frequency dispersion and dissipation. Finer grid spacing is created near shore, in shallow water, where the wavelengths are shorter and local irregularities in bathymetry, hence wave progagation speed and refraction, are important. The initial condition, coseismic sea surface displacement, was located according to the geophysical data, fault and seafloor mapping, in geographic coordinates and translated to the bathymetric and topographic grid. The initial surface displacement was modeled using the seismic parameters for the seven segment fault model shown in Table 1.

Table 3. Synthetic Wave Gauge Parameters (see Fig. 9 for locations).

Name	Symbol	Depth (m)
Point Dume	dume	19.2
Marina del Rey	mdr	9.8
King Harbor	kh	12.1
Palos Verdes	pv	23.8
LA/LB Harbor	lalb	9.8
Anaheim Bay	ana	10.3
San Onofre	sano	10.3
Avalon	ava	57.8

Figure 10 shows the location of the initial surface displacement and the computed run-up along the south-facing and west-facing shorelines. Note that these data are uncorrected for the local tidal

variations, so that actual run-up would be increased (or decreased) by the effective tidal water levels (another 1-2 m) at the time the tsunami reaches the coast. Run-up values are highest along the San Pedro Bay and Santa Monica Bay coasts with run-up heights exceeding two meters in the vicinity of the Los Angeles and Long Beach harbors. Concentrations of higher run-up occur along the coast in the vicinity of Marina del Rey, King Harbor and Redondo Beach, the Los Angeles and Long Beach harbor area, and the Newport Beach area. Run-up heights exceed one meter for most of the coast between Santa Monica and Dana Point.

Synthetic wave-gauge records are shown for locations along the coast (Table 3; Figs. 9 & 11). The wave gauge records show water surface fluctuations that vary from 1-2 meters, peak-to-peak, that begin with a leading sea surface rise about 10-18 minutes after the wave was generated. The initial water motion takes from 5-10 minutes to complete and the wave motions persist for more than 40 minutes, after which time the simulation was terminated. Such long period oscillations have the potential to generate substantial currents in the narrow openings of harbors—a phenomenon observed in other tsunamis (Borrero et al., 1995). Although the entrance to the Los Angeles and Long Beach harbors are south and east facing, refraction of the waves focuses the tsunami energy in this area. Much more detailed studies are needed, however, to accurately assess the impact of this tsunami source on the Los Angeles and Long Beach harbors and the marine facilities located therein.

Wave periods are generally shorter, about 3-5 minutes for wave gauges along open coast areas with narrow shelves and steep submarine escarpments like Point Dume, Palos Verdes, San Onofre and Avalon. The large short period initial wave heights at Palos Verdes and Avalon probably result from amplification of the leading tsunami wave front up as it crosses the steep submarine escarpment and crosses the narrow shelf. Marina del Rey, King Harbor, and the Los Angeles/Long Beach harbor gauges show a similar high amplitude initial wave, at somewhat longer period. These sites also show a second large wave arriving 15-20 minutes after the first large wave. The second wave run-up exceeds the first for both King Harbor and the Los Angeles/Long Beach harbor gauges, but is slightly smaller for Marina del Rey. A second set of larger waves also arrives at Palos Verdes, but with a longer delay, about 25-30 minutes after the initial wave set, and with about one-third the amplitude of the biggest peak in the first set. Note that the biggest wave is the second wave in the first set at Palos Verdes, arriving about 5-10 minutes after the initial wave. These later arriving waves are presumably due to wave dispersion across the slope and shelf and should remind us that the first wave in any tsunami is often not the largest or most dangerous.

The tsunami generated by the fault model used in this study actually consists of two somewhat independent wave fronts radiating from the northwest and southeast ends of the submerged island uplift

(Fig. 12). The tsunami separates into these two wave fronts because the highest point of uplift is subaerial, occurring near the middle of the island and does not contribute directly to tsunami generation (Fig. 8). As the two wave fronts propagate toward the coast, their interaction forms areas of constructive and destructive interference with local amplification and de-amplification. Wave amplification due to constructive interference occurs most strongly at the southern tip of the Palos Verdes peninsula near San Pedro, although wave refraction due to changing bathymetry modifies this interaction and creates larger amplifications to the east from the Los Angeles and Long Beach harbors to Anaheim Bay and Newport Beach. Wave refraction further amplifies the run-up at places like Marina del Rey and Anaheim Bay due to a wave-guide effect of westward projecting shelf areas and due to a gently concave coastline acting to funnel the wave energy as occurs at Hilo, Hawaii, but to a lesser degree.

Anaheim Bay is the last major coastal area to be struck by the tsunami, with the first arrival occurring 10-15 minutes after the wave arrival at Palos Verdes or Point Dume. Later arrivals at some major coastal harbor facilities could allow a more effective warning to people in those areas. For example, wave gauges placed at strategic places along the coast where any distant or offshore tsunami would strike first, due to the deeper water and faster wave speeds, could provide warnings to the harbor areas located across the relatively broad shelf areas where the tsunami is slowed substantially. Thus, wave gauges at Point Dume, Palos Verdes, and Laguna Beach areas could provide several minutes advance warning. Of course, deep water gauges similar to those installed for the Pacific Tsunami Warning Center, but located closer to the active Borderland faults, could provide even more advance warning, but may not observe the full wave amplification expected at the coast.

SOURCE VARIABILITY

A single scenario fails to account for the highly variable nature of earthquake and tsunami phenomena. So, we ran additional earthquake source models to measure the variability in tsunami run-up due to large earthquakes on the Catalina fault. For the present study, six sub-events, comprised of one or more fault segments derived from the full seven segment model were modeled (Figs. 13-14, Table 4). A more thorough analysis could include a Monte Carlo (stochastic) simulation utilizing a large number of potential events with varying fault rupture parameters and associated seafloor deformation and tsunami generation (cf., Geist, 2002). Such an analysis was beyond the scope of this project, and the seven scenarios modeled are believed to provide a representative measure of the range of run-up that may be expected from large earthquakes on the Catalina fault zone. Furthermore, because these sub-events span the different submarine segments of the Catalina fault zone on both ends of the island, the effects of wave refraction in amplifying run-up along the adjacent coast may be distinguished from the effects of source location. In particular, we verify that large earthquakes on the northwestern fault segments create higher run-up in Santa Monica Bay whereas large earthquakes on the southeastern fault segments create higher run-up in San Pedro Bay and along the Orange County coast as expected simply from geographical proximity.

Table 4. Earthquake Scenarios for Tsunami Generation Along Santa Catalina Uplift

Segments*	Length (km)	Fault Area (km^2)	Max. Slip (m)	Ave. Slip (m)	Magnitude (M_w)	Max. Uplift (m)
1-7	164.546	2317.35	6.4	4.461	7.63	2.169
1-4	86.536	1225.2	5.0	4.386	7.44	2.168
5-7	78.010	1092.1	6.4	4.544	7.41	1.433
1-4	86.536	1225.2	3.6	2.610	7.29	1.303
2-4	64.604	918.16	3.6	1.500	7.04	0.710
5-7	78.010	1092.1	6.4	2.610	7.25	1.391
5-6	48.311	676.36	2.0	1.917	7.02	0.461

*See Table 2 for segment parameters

The uplift of the Santa Catalina Island platform most likely results from many large earthquakes over thousands to millions of years of geological time. Geological investigations show that marine sedimentary rocks and fossils now found elevated on the island were originally deposited at abyssal depths, as much as 2,000 meters below sea level, during late Miocene time (about 6-10 Ma). The full seven segment earthquake fault rupture scenario (case 1) modeled to reproduce the general shape of the Santa Catalina Island uplift provides an estimate for a maximum magnitude event. The slip for the fault segments was scaled to representative values consistent with empirical data on fault slip versus fault rupture length and earthquake magnitude (Wells and Coppersmith, 1994). Uniform slip on each planar

fault segment is varied along strike to produce the pattern of uplift observed in the island platform geomorphology (Fig. 8).

Although a characteristic earthquake model may be appropriate for the Catalina fault zone, available data are inadequate to test such a model. It is likely, however, that there are many different large "characteristic" earthquake events that combine through geologic time to produce the uplift of the island platform. The six sub-events (Fig. 13, Table 4) provide a suite of events that represent the magnitude range (M_w=7.0-7.6) of events large enough to produce potentially destructive local tsunamis, yet are scaled appropriately to reproduce the shape of the island platform morphology. The slip parameters used for each model were scaled down for the shorter fault rupture lengths associated with the smaller sub-events, and are consistent with empirical maximum slip and average slip values versus fault rupture length and magnitude observed in historic earthquakes.

Coastal run-up produced by the seven different earthquake scenario tsunamis shows patterns consistent with source geometry, earthquake magnitude, and wave refraction due to irregular bathymetry and coastal configuration (Fig. 14). The scenarios involving rupture of the northwestern fault segments tend to produce higher run-up in Santa Monica Bay and those involving rupture of the southeastern fault segments produce higher run-up in San Pedro Bay and along the Orange County coast. Case 2 involves the entire four segments of the southeast fault section whereas case 3 involves the remaining three segments of the northwest fault section. The coastal run-up patterns match the relevant sections of the full 7-segment scenario except that the amplified run-up in the middle, from Long Beach to Newport Beach, is reduced. This confirms our conclusion that the constructive interference between the two separate wavefronts produced by the full 7-segment rupture amplifies the wave heights at the coast in this area. Coastal run-up for the other four earthquake scenarios produce similar patterns to those of the northeast or southwest sections at reduced amplitudes commensurate with the smaller magnitude and vertical displacements (Fig. 14). In general, the maximum run-up values along the coast are roughly one-half the values for the larger earthquake scenarios.

To separate the effects of earthquake magnitude from tsunami wave refraction for the different scenarios, a second plot of run-up along the coast was made with run-up values normalized to the maximum uplift produced in the elastic dislocation model (Fig. 15). The overall shape of the run-up plots are similar for the absolute run-up and normalized run-up cases, with peaks located at the harbor areas described above. This implies that these peaks are due to wave refraction effects and that any large tsunami, from local or distant sources, may be amplified in these same areas. Indeed, the tsunami from the 1960 Chilean (M_w=9.5) earthquake was strongly amplified in the Marina del Rey area where the waves exceeded the height of the tide gauge (1.6 m amplitude measured) and persisted with high

amplitudes (> 1 m) for more than ten hours (Lander et al., 1993). The location of Marina del Rey, near the center of the semi-enclosed Santa Monica Bay, may suffer a natural wave resonance condition. An alternative explanation may be that the westward projecting shallow water area (Shelf Projection Anticlinorium, Nardin and Henyey, 1978) bounded between Santa Monica and Redondo submarine canyons acts as a tsunami wave-guide that focuses energy into the Marina del Rey and King Harbor areas. Wave heights are also amplified around the northwestern end of the Palos Verdes peninsula, possibly due to similar refraction effects but also because of less attenuation due to the shorter distance from the fault rupture source. Previous tsunami hazard studies along the southern California coast (Houston, 1980; McCulloch, 1989) show similar patterns of amplification in Santa Monica Bay (from Santa Monica to Redondo Beach) and San Pedro Bay (from Los Angeles Harbor to Newport Beach) with less amplification at the Palos Verdes peninsula. These older studies were based on distant tsunami sources, from Alaska or South America, so that the geometrical spreading attenuation effects are reduced for the long period waves once they reach the local southern California coastal area (plane wave approximation?).

Normalized run-up plots show that the maximum amplification of tsunami wave height along the coast is less than 150 percent (Fig. 15). The run-up computed with the MOST program is for a smoothed coastline and bathymetric model (400 meter grid) so that local amplification at higher spatial frequencies may be smoothed out. In general, coastal run-up lies between 50-150 percent of the maximum tectonic uplift due to the fault rupture. Consequently, if local high-slip patches occur with greater seafloor uplift than predicted from the simple elastic dislocation model, adjacent coastal areas may have run-up values at similar levels. Our models predict coastal run-up ranging from 0.5-2.5 meters for offshore earthquakes at magnitude 7.0-7.6 levels. Conservatively assuming a factor of two uncertainty for the reasons discussed previously, local tsunamis from earthquakes along the Catalina fault system may produce coastal run-up from 1-5 meters in elevation. If the variability can reach a factor of 6.5 as found by Geist (2002) for stochastic simulations of Cascadia subduction earthquakes, then it is conceivable that maximum run-up from large local tsunamigenic earthquakes offshore southern California may exceed 10 meters.

Because the Catalina fault system is predominately strike-slip in character, the maximum seafloor uplift may be reduced compared to other southern California fault systems where thrust or reverse faulting predominates. Roughly equal partitioning between strike-slip and dip-slip was observed in the 1989 Loma Prieta earthquake within the predominately right-slip San Andreas fault system (Plafker and Galloway, 1989). Thus, we may expect similar partitioning along the Catalina fault system. Large strike-slip earthquakes may still produce destructive tsunamis as observed during the 1992 Mindoro,

Philippines earthquake (Daag et al., 1995) where maximum run-up reaching 8.5 m was produced by a large strike-slip earthquake (M=7.1).

Limitations of the Model

Notwithstanding our attempts to more realistically model the earthquake source for tsunami generation, the models developed are still quite simple compared to actual observed earthquake fault rupture parameters (cf., Wald and Heaton, 1994). Our simple models involve planar rectangular fault segments with uniform slip for each segment, whereas the distribution of slip within real earthquakes is more complex with local areas of high slip that often have irregular geometry. Often, there may be several active faults involved in one large earthquake, such as the 1992 Landers earthquake (M_w=7.3) with complex distributions of slip on each segment. Lastly, variability of the slip distribution from one characteristic earthquake to the next on a particular fault is also observed in real earthquakes such as the 1940 Imperial Valley and 1979 El Centro earthquakes on the Imperial fault (Sharp, 1982; USGS, 1982). We believe that our simple models provide an adequate representation of real earthquake variability with regard to the wavelengths and scales involved in local tsunami generation. Thus, although more complex models of the slip distribution for the faulting in each earthquake scenario could be developed, the details of the fault rupture tend to be smoothed out at the seafloor vertical displacement and initial tsunami wave height in the elastic dislocation model.

One area of concern is that the elastic dislocation model produces relatively smaller vertical displacements than the maximum fault slip on the modeled fault surfaces. This result may be reasonable for buried fault sources where no surface rupture occurs (e.g., 1989 Loma Prieta earthquake, Plafker and Galloway, 1989). However, where surface fault rupture, or for submarine earthquakes, seafloor fault rupture, the maximum surface displacements often equal or approach the maximum subsurface displacement values derived through seismological observations (cf., Wald and Heaton, 1994; Treiman et al., 2002). Seafloor fault scarps of similar height, likely resultant from prehistoric large earthquakes, have been observed on major faults offshore southern California (Goldfinger et al., 2000). Because we typically observe only about one-half the maximum subsurface slip value as surface displacement in the elastic dislocation model, we propose that our estimates of seafloor uplift and initial tsunami wave height may be too low by a similar amount (about 50 percent). This proposition appears to be supported by observations of recent tsunamis around the world where the measured maximum run-up values also tend to be about twice the predicted values from elastic dislocation models of tectonic faulting based on seismological observations (cf., Geist, 2002).

Landslide versus Earthquake Tsunami Sources

The run-up values predicted in this study ignore the possibility of large submarine landslides being triggered by the earthquake. Larger run-up associated with large submarine landslides has been estimated in recent studies (Synolakis et al., 2002), but this study focuses on the tectonic sources only. The schist basement of Santa Catalina and adjacent offshore areas is prone to landsliding (Vedder et al., 1979) and large-scale basement-involved landslides have been mapped in the southern California offshore area (Legg and Kamerling, 2002). A large earthquake on the Catalina fault system could generate a large landslide that affects the steep submarine slopes around the island and generate additional tsunami wave energy to that of the tectonic displacement. Further research is needed to examine this possibility and estimate the wave height and run-up expected from realistic submarine landslide sources around the island.

Although numerous submarine landslides have been mapped in the California Continental Borderland (Greene and Kennedy, 1987; Field and Edwards, 1980; 1993; Legg and Kamerling, 2002), large possibly catastrophic submarine landslides appear to be relatively rare. For example, the large basement-involved landslide described by Legg and Kamerling (2002) appears to be more than 100 ka, and the large San Pedro Canyon submarine landslide is about 7,500 years old (M. Fisher, personal communication, 2002). Estimated slip rates along the major offshore fault zones range from about 1 mm/yr for the Newport-Inglewood-Rose Canyon fault zone (Fischer and Mills, 1991; Lindvall and Rockwell, 1995) to about 3 mm/yr for the Palos Verdes fault zone (McNeilan et al., 1993; Ward and Valensise, 1994) or possibly greater than 5 mm/yr for the San Clemente fault zone (Legg, 1985; 1991). Large earthquakes, with M>7 involving slip of 1-6 meters would have recurrence times of a few hundred to a few thousand years, substantially shorter than the apparent frequency of large submarine landslides in the borderland. Consequently, the first order driving force for locally generated tsunamis offshore southern California is expected to be tectonic deformation from large earthquakes.

Tsunami Recurrence and Statistics

For the suite of earthquake scenarios modeled in this study, a first order estimate of local tsunami recurrence may be prepared. The following assumptions and limitations must be considered in this analysis:

1) Only the faulting responsible for the uplift of the Santa Catalina Island platform has been modeled, so the analysis is limited to this potential source;
2) The slip rate for the Catalina and San Diego Trough fault zones, which comprise the principal faults modeled for this study, is unknown and must be assumed at this time;

3) Only a small set of potential earthquake scenarios for the Catalina fault system were modeled, but these are believed to represent the range of potential tsunami heights that may be produced by earthquakes in the M=7.0-7.6 range for this fault system;
4) Tsunamis produced by earthquake-induced submarine landslides are not considered in this analysis, but these are believed to be sufficiently rare (for the large tsunamigenic landslides) to represent worst-case events and not the nominal 100-year or 500-year occurrences;
5) The elastic dislocation model may systematically underestimate the seafloor uplift that may occur during real earthquakes with seafloor fault rupture similar to the observed subaerial fault rupture in recent earthquakes;
6) The bathymetry and coastal topography are modeled on a 400-meter grid and smoothed along the coast to avoid high-frequency instabilities in the long-wave propagation code so that local anomalies in run-up may be missing from the analysis.

In spite of these limitations, this study can provide a first order estimate of the frequency and probability of occurrence for locally generated tsunamis in the southern California area.

The Santa Catalina Island uplift is one of the largest elevated structures in the Inner Borderland of southern California, south of the Transverse Ranges. Therefore, tsunami hazards from tectonic displacements along the Catalina fault system may represent the most severe local tsunami hazard source region neglecting submarine landslide sources. A conservative approach is to consider the tsunami run-up levels modeled for the Santa Catalina Island uplift and Catalina fault system, and estimate recurrence times based on the overall slip rate for offshore fault systems in southern California. No published estimates of the slip rate for the Catalina fault system are available at this time. Based on the well-defined character of the Catalina and San Diego Trough fault zones, the slip rate is likely to be similar to that of other well-defined fault zones in southern California such as the Palos Verdes and Newport-Inglewood-Rose Canyon fault zones where slip rates are measured at 1-3 mm/yr (Fischer and Mills, 1991; McNeilan et al., 1993; Valensise and Ward, 1994; Lindvall and Rockwell, 1995). Furthermore, the Santa Cruz-Catalina Ridge fault zone splits into the Catalina and San Clemente fault zones at the northern end of the island uplift. Preliminary estimates of slip rates for the San Clemente fault zone south of San Clemente Island are 4-7 mm/yr (Legg, 1985). Geodetic estimates of present-day tectonic plate motions suggest that as much as 20 percent of the Pacific-North America relative motion occurs offshore southern California (Bennett et al., 1993; Larson, 1993; Demets and Dixon, 1999; Sella et al., 2002), or roughly 10 mm/yr.

Only a small set of potential earthquake-generated tsunamis are modeled in this study, and so the full range of potential scenarios for local southern California tsunamis may be poorly represented. Geist

(2002) shows that the complexity in real earthquakes may preclude use of a few simplified elastic dislocation models to successfully model the natural variability in tsunami amplitudes. He finds that peak nearshore tsunami amplitudes can vary by a factor of 2.5 or more based on stochastic modeling of Cascadia subduction zone interplate thrust earthquakes. We may assume similar variability for earthquakes of a specific magnitude on the Catalina fault system. Indeed, variability within our suite of seven scenarios approaches a factor of 5.0 for an earthquake magnitude range of about 0.6, and tsunami amplitudes vary by a factor of 1.5 for a given magnitude (Table 4). For the conservative assumption that the elastic dislocation models used underestimate the maximum tsunami run-up by a factor of 2.0, the range of variability expected for realistic earthquake-generated local tsunamis in southern California is believed to be adequately represented for this first order hazard assessment.

Large earthquakes on the offshore fault systems are the most likely triggers for large-scale submarine landslides in the region. Nevertheless, large earthquakes on coastal or onshore fault systems like the San Andreas may be sufficient to trigger submarine landslides offshore, such as occurred in Monterey Bay during the 1989 Loma Prieta earthquake (Schwing et al., 1990; McCarthy et al., 1993). Current data suggest that large submarine landslides are rare events, with recurrence times measured in several thousand to hundred thousand years (M. Fisher, personal communication, 2002, Legg and Kamerling, 2002). Therefore, for commonly used hazard recurrence times of 100 years and 500 years (cf., Houston, 1980; McCulloch, 1985), the large landslide-generated tsunamis are on the very long return period tail of the probability distribution. Considering the other conservative assumptions described above, the preliminary estimate of recurrence times for locally generated tsunamis in southern California provided herein is reasonable for the short-term probabilities. More detailed, site-specific analyses for high-risk facilities such as nuclear power plants are necessary to accurately assess the local tsunami hazard at long time intervals and low probabilities.

Two methods based on average displacement rates are used to estimate the occurrence frequency of the large earthquakes modeled, and the associated local tsunami hazard. The first method is commonly used in paleoseismic analyses, assuming a characteristic earthquake model and dividing the average event slip by the average fault slip rate to derive a recurrence interval. The second method recognizes that natural complexity in earthquake fault rupture results in some earthquakes with mostly strike-slip mechanisms and others with significant dip-slip mechanisms. For example, the 1906 San Francisco earthquake ruptured through the Santa Cruz Mountains restraining bend uplift, but may have been mostly strike-slip in character, whereas the 1989 Loma Prieta earthquake was about equally partitioned between strike-slip and dip-slip (Plafker and Galloway, 1989). Thus, a more accurate estimate of recurrence times for locally generated tsunami may be provided by dividing the maximum uplift for the earthquake

scenario divided by the average rate of uplift of the Santa Catalina Island platform. Similar analyses have been made for uplift of the Palos Verdes Hills to estimate the slip rate on the Palos Verdes fault zone (Ward and Valensise, 1994) and for uplift of the Santa Cruz Mountains (Valensise and Ward, 1990).

Using a simple assumed slip rate of 1 mm/yr for right-slip along the Catalina fault system, the recurrence time large ($M \geq 7$) earthquakes in the Santa Catalina Island uplift area would be about 1,500-4,500 years (from Table 4, 1.5-4.5 m average slip divided by 1 mm/yr average slip rate). If the maximum rate of right-slip for the offshore region is used, about 10 mm/yr, then the recurrence time is reduced accordingly by an order-of-magnitude to 150-450 years. No earthquakes of this magnitude have been recorded in the brief history of the southern California region, although possible large earthquakes, approaching M=7 occurred offshore Oceanside area on November 22, 1800. Farther north, a large earthquake struck the Santa Barbara Channel area on December 21, 1812, and offshore Point Arguello on November 4, 1927. Grant et al (2002) suggest that the 1769 earthquake felt by the Portola expedition occurred along the coastal fault system near Newport Beach. Thus, recurrence times of a few hundred years for M~7 earthquakes offshore southern California may be a reasonable first order estimate. Recurrence times of a several hundred to a few thousand years for M>7 earthquakes on the Catalina fault with significant seafloor uplift and local tsunami generation seems appropriate.

The total structural relief across the Catalina fault system measures about 650 m elevation for Mt. Orizaba, plus 1,300 m water depth at the base of the escarpment, plus about 300 m of basin fill below the escarpment (Vedder, 1987) to total at 2,250 meters. Geological studies show that the Santa Catalina Island area has been elevated at or above sea level in middle Miocene time, when most of the volcanic rocks on the island were emplaced (Vedder et al., 1979), then subsided rapidly at the end of Miocene into early Pliocene time reaching abyssal depths in some areas (2,000 m). Thus, uplift of the Santa Catalina Island platform to its present elevation occurred since early Pliocene time, within the last 3-6 Myrs B.P. Other prominent southern California features have been uplifted in this same time period including the Palos Verdes Hills (Nardin and Henyey, 1978). An average rate of tectonic uplift for the Santa Catalina Island block is 0.375-0.75 mm/yr. Measured rates of tectonic uplift in the southern California coastal area range from 0.1-0.4 mm/yr based upon studies of elevated Pleistocene marine terraces on the coast and offshore islands (Lajoie et al., 1992), with somewhat higher rates measured (about 3 m/ka) near Ventura and Cape Mendocino where active faulting has more significant vertical motions. Assuming that uplift of Santa Catalina Island occurred tectonically through large earthquakes as we have modeled above, the estimated recurrence times for M=7.0-7.6 events on the Catalina fault system is about 600-6,000 years (1,000-9,000 years including subsidence). Other large seismogenic faults in the Los Angeles

and southern California area have similar long recurrence times based upon paleoseismic studies including the Sierra Madre fault (Tucker and Dolan, 2001) and faults of the Eastern California Shear Zone (Rockwell et al., 2000). McNeilan et al., (1996) estimate recurrence intervals for large (M>7) earthquakes on the Palos Verdes fault zone at about 400-1,400 years using a measured right-slip rate of 2.7-3.0 mm/yr. If our earthquake models and uplift rates of Santa Catalina Island are reasonable, then the slip rate on the Catalina fault system appears to be about five times slower (<1 mm/yr) than that of the Palos Verdes fault zone. The estimated rate of uplift for the Palos Verdes Hills, however, is less than one-half the value we have assumed for Santa Catalina Island. As noted by Ward and Valensise (1994), folding associated with a buried oblique-reverse fault creates variable uplift rates across the growing structure. Furthermore, the rate used herein for the uplift of the Santa Catalina Island restraining bend includes both the uplift of the island and the subsidence adjacent to the island on the footwall of the Catalina fault. Lastly, Ward and Valensise (1994) modeled a deeply buried, blind, oblique-reverse fault that lies six kilometers below the ground surface, whereas our model of the Santa Catalina Island uplift extends faulting to within 0.5-1.5 km of the surface. As our model testing showed, deeper blind faults produce broader uplift with lower amplitudes than shallow faults. Therefore, we conclude that our preliminary estimates of the uplift rate, and hence, rough earthquake recurrence estimates are reasonable and consistent with rates measured or estimated for other major faults in the southern California region.

Ward and Valensise (1994) concluded that M=6.75 represented a maximum magnitude for the Palos Verdes fault, and their analysis suggested an average slip for such an event of 3.7 m. In contrast, our analysis finds that a similar average slip is more consistent with larger earthquakes, M_w=7.4-7.6 (Table 4), which involves a greater length of faulting than the 19 km long by 7 km wide blind fault modeled under the Palos Verdes Hills. Indeed, we suggest that Ward and Valensise (1994) have seriously understated the earthquake potential of the Palos Verdes fault zone, primarily due to ignoring the shallow part of the fault zone as well as its greater lateral continuity offshore in Santa Monica and San Pedro Bays. Our fault rupture models for the Catalina fault system include, both the relatively shallower, but still high-angle, right-oblique reverse fault segments, as well as the near vertical predominately right-slip fault segments.

It is uncertain whether large earthquakes with some areas of oblique-slip can rupture completely through major restraining bends like the Santa Catalina Island uplift, or whether oblique strain is partitioned between large strike-slip earthquakes on the near vertical fault sections and smaller, but still potentially destructive oblique-reverse earthquakes on the moderately-dipping fault segments within the bend. Strain partitioning appears to occur along the Santa Cruz Mountains restraining bend of the San Andreas fault in northern California. The 1989 Loma Prieta earthquake accommodated oblique-reverse

movement on a blind fault beneath the mountain crests, and the 1906 San Francisco earthquake accommodated predominately right-slip along the entire northern California section of the San Andreas fault. Sibson (1985) proposed that large earthquakes may initiate or terminate at releasing step-overs within major fault zones. Historical earthquakes such as the 1857 Fort Tejon earthquake on the San Andreas fault appears to have terminated at a significant releasing step-over in the Cajon Pass area. Here, the San Jacinto fault splits from the San Andreas and the San Andreas principal displacement zone (PDZ) may step south to the Banning fault. We model a similar releasing step-over within the Santa Catalina Island restraining bend. Paleoseismic evidence suggests, however, that some great (M>7.5) earthquakes on the southern San Andreas fault zone may break all the way through the Cajon Pass and San Bernardino Mountains segment to the Salton Sea along the Coachella Valley segment (Sieh et al., 1989). Our tsunami modeling has considered both types of scenario.

SUMMARY and CONCLUSIONS

To evaluate the potential for destructive tsunami generated by local earthquakes offshore southern California, we model the Santa Catalina Island restraining bend with a realistic fault geometry and oblique-reverse earthquake displacement field to match the overall shape of the island block morphology. We successfully reproduced the shape of the Santa Catalina Island platform uplift using a 164-km long, seven segment, elastic dislocation fault model with a maximum displacement of 6.4 meters (M_w=7.6, Table 2; Figure 8). The displacement on each fault segment was adjusted in both right-slip and reverse-slip components to produce the uplift pattern with the displacement amplitudes scaled to realistic values for large earthquakes ($M \geq 7$). To estimate the variability of potential earthquakes and seafloor displacement, a suite of six sub-events, M_w=7.0 to7.4 (Table 4) were modeled using various combinations of the seven fault segments. Segment displacements were scaled to values appropriate for the fault rupture length and earthquake magnitude while maintaining the relative proportions of right-slip and reverse-slip of the 7-segment model that produce the overall shape of the Santa Catalina Island uplift. The vertical displacement produced by the elastic dislocation model was used as a static displacement initial condition for the sea surface representing co-seismic generation of a tsunami. Although maximum tectonic uplift varied from about 0.5-2.2 meters, the initial wave height was somewhat less because the highest uplift occurs on the subaerial part of the island. Maximum subsidence on the footwall block southwest of the Catalina escarpment exceeded 1.3 m. The presence of the island effectively separates the initial sea surface elevation into two northwest trending wave fronts. The waves were propagated toward the adjacent southern California coast using a long period hydrodynamic wave model (MOST, Titov and Gonzalez, 1997) to compute the expected coastal run-up. Bathymetry for the shallow water wave propagation was derived from NOAA surveys in the region gridded to a 400-m horizontal spacing and smoothed somewhat along the coast to avoid numerical instabilities. Significant run-up was measured along the southern California coast from Point Mugu to Solana Beach at the ends of the bathymetry grid. Maximum run-up exceeded one meter along most of the coast between Santa Monica and Dana Point, with peaks of 1.5-2.2 m at Marina del Rey, Redondo Beach, Los Angeles and Long Beach harbors, and the Orange County coast from Seal Beach to Newport Beach. These areas most severely affected also correspond to the major harbor areas where marine terminals and boating facilities are located in harm's way. Experience from historical distant tsunamis such as generated by the 1960 Chilean and 1964 Alaskan earthquakes show these harbor areas to be vulnerable to strong currents that scour pilings and smash boats. Recent observations of tsunami run-up around the world following large earthquakes tend to show that run-up values predicted from simple elastic dislocation models of tectonic deformation may underestimate the actual peak run-up values by a

factor of two. Complex interactions between the tsunami wavefield and local bathymetry and coastal configuration may create locally severe wave amplification and run-up. Consequently, actual coastal run-up values from large earthquakes on the Santa Catalina Island restraining bend may exceed 2-4 m. Travel time between the earthquake occurrence and arrival of the first waves at the adjacent coast varies from 10-20 minutes for the areas most severely affected, much shorter for locations on the island, so that no official warnings could be broadcast in sufficient time for evacuation. The strong earthquake may provide the only warning to affected coastal residents, and concurrent quake-related damage, including potential widespread liquefaction and failures of oversteepened coastal bluffs, may exacerbate evacuation or rescue efforts. Fortunately, large earthquakes on this major offshore fault system appear to be infrequent, with estimated recurrence intervals measured in several hundred to thousands of years. However, if clustering of events is characteristic of major fault systems offshore southern California, as has been interpreted for several onshore fault systems, the local tsunami hazard may be enhanced during the cluster period. Some have suggested that an ongoing surge of activity along the coastal fault system may represent such a cluster that currently affects the southern California and northern Baja California coastal zone. Further research is needed to measure slip rates on the major offshore fault systems and try to identify the frequency and magnitude of large prehistoric submarine earthquakes that may have generated potentially destructive local or regional tsunamis. Likewise, direct geological investigations to identify possible prehistoric tsunami deposits along the southern California coast are needed to quantify more accurately this offshore threat. Meanwhile, coastal construction including major marine terminals, power plants and other important coastal facilities should pro-actively evaluate their local tsunami threat, structural and human vulnerabilities, and level of exposure to provide more accurate risk assessment and begin to implement effective risk reduction measures.

Tsunami potential and coastal run-up predicted by our modeling of the Santa Catalina Island restraining bend appears consistent with historical observations in the region. The maximum run-up predicted is generally 1-2 meters over much of the southern California coastal area, roughly equivalent to that observed following the November 4, 1927 Lompoc earthquake on the nearby south central California coast (Lander et al., 1993). Our run-up estimates may understate the coastal run-up due to amplification by local irregularities in the coastal bathymetry and configuration, or due to understating the seafloor uplift by using an elastic dislocation model. We believe that the run-up due to the tectonic deformation may be about a factor of two greater than our estimates. Thus, the tsunami amplitudes are comparable to the highest tidal ranges. Nevertheless, because there are multiple wave crests that strike the coast, some are likely to hit during high tides and therefore have the potential for serious destruction. Winter storm surf and swell coupled with high astronomical tides already create havoc in many of the

low-lying coastal areas such as Seal Beach. Furthermore, the strong currents that are generated by the rapidly changing sea level during the tsunami attack, with wave periods of about 10-20 minutes, have been destructive to boats and moorings and other harbor facilities during past distant tsunamis such as the 1960 Chilean and 1964 Alaskan events. Consequently, the hazard posed by locally generated tsunami attack is very serious and should be appropriately mitigated. Lastly, this study only examined the tectonic deformation from large earthquakes as potential tsunami source. Large-scale submarine landslides represent a serious threat, and the large earthquakes we have modeled would very likely trigger widespread slope failures, both subaerially along the coasts and submarine landslides along the steep borderland slopes. The 1994 Papua New Guinea tsunami of landslide origin shows that in the near source area (landslide area), landslide generated tsunami run-up may greatly exceed that from tectonic deformation. A realistic earthquake scenario should consider that both the tectonic source and landslide sources of local tsunami may occur.

REFERENCES

Barka, A., and 21 others, 2002. The surface rupture and slip distribution of the 17 August 1999 Izmit earthquake (M 7.4), North Anatolian fault, *Bulletin of the Seismological Society of America*, v. 92, p. 43-60.

Bennett, R.A., Rodi, W., and Reilinger, R.E., 1996. Global Positioning System constraints on fault slip rates in southern California and northern Baja, Mexico, *Journal of Geophysical Research*, v. 101, p. 21,943-21,960.

Bohannon, R. G., and Geist, E., 1998. Upper crustal structure and Neogene tectonic development of the California Continental Borderland, *Geological Society of America Bulletin*, v. 110, p. 779-800.

Bohannon, R., Eittreim, S., Childs, J., Geist, E., Legg, M., Lee, C., Sorlien, C., and Busch, L., 1990. A seismic-reflection study of the California Continental Borderland, [abstract] in *Trans. American Geophysical Union*, v. 71, p. 1631.

Borrero, J., Ortiz, M., Titov, V., and SYnolakis, C., 1995. Fiedl survey of Mexican tsunami produces new data, unusual photos, *EOS, Trans. American Geophys. Union*, v. 88, p. 87-88.

Christie-Blick, N., and Biddle, K. T., 1985. Deformation and basin formation along strike-slip faults, in Biddle, K.T., and Christie-Blick, N., editors, 1985, *Strike-Slip Deformation, Basin Formation, and Sedimentation*, Society of Economic Paleontologists and Mineralogists *Special Publication No. 37*, p. 1-34.

Clarke, S. H., Greene, H. G., Kennedy, M. P., and Vedder, J. G., 1987. Geologic map of the inner-southern California continental margin, California Division of Mines and Geology, *California Continental Margin Geologic Map Series*, Area 1 of 7, sheet 1 of 4, scale 1:250,000.

Corbett, E. J., 1984. Seismicity and crustal structure studies of southern California: Tectonic implications from improved earthquake locations, [Ph.D. dissertation] California Institute of Technology, Pasadena, California, 231 p.

Crouch, J. K., and Suppe, John, 1993. Late Cenozoic tectonic evolution of the Los Angeles basin and inner California borderland, A model for core complex-like crustal extension: *Geological Society of America Bulletin*, v. 105, p. 1415-1434.

Crowell, J. C., 1974. Origin of late Cenozoic basins in southern California, *in* Dickinson, W. R. (Editor) Tectonics and sedimentation, Society of Economic Paleontologists and Mineralogists, *Special Publication 22*, p. 190-204.

Daag, A.S., De los Reyes, P.J., Tubianosa, B.S., Javier, D.V., and Punongbayan, R.S., 1995. Tsunami deposit of the 15 November 1994 Mindoro earthquake, Philippines. *Proceedings, Tsunami Deposits, Geologic Warnings of Future Inundation*, University of Washington, Seattle, 22-23 May, 1995, p. 3.

DeMets, C., and Dixon, T. H., 1999. New kinematic models for Pacific-North America motion from 3 Ma to present, I: Evidence for steady motion and biases in the NUVEL-1A model, *Geophysical Research Letters*, v. 26, p. 1921-1924.

Field, M.E., and Edwards, B. D., 1980. Slopes of the southern California borderland: A regime of mass transport, *in* Field, M.E., Bouma, A.H., Colburn, I.P., Douglas, R.G., and Ingle, J.C. editors, Los Angeles, Pacific Section SEPM, *Pacific Coast Paleogeography Symposium No. 4*, p. 169-184.

Field, M.E. and Edwards, B.D., 1993. Submarine landslides in a basin and ridge setting, southern California, *in* W.C. Schwab, H.J. Lee and D.C. Twichell,.editors, *Submarine landslides; selected studies in the U.S. Exclusive Economic Zone*, Denver, U.S. Geological Survey, *Bulletin 2002*, p. 176-183.

Fischer, P. J., and Mills, G. I., 1991. The offshore Newport-Inglewood - Rose Canyon fault zone, California: Structure, segmentation, and tectonics, *in* Abbott, P.L., and W.J. Elliott (Editors) *Environmental Perils of the San Diego Region*, San Diego Association of Geologists Guidebook, p. 17-36.

Geist, E. L., 1998. Local tsunamis and earthquake source parameters, in *Tsunamigenic Earthquakes and Their Consequences, Advances in Geophysics*, v. 39, p. 117-209, Academic Press, San Diego.

Geist, E. L., 2002. Complex earthquake rupture and local tsunamis, *Journal of Geophysical Research*, v. 107, p. ESE 2-1-16.

Goldfinger, C., Legg, M., and Torres, M., 2000. New mapping and submersible observations of recent activity on the San Clemente fault, *EOS, Trans. American Geophysical Union, 81,* 1069.

Grant, L. B., Ballenger, L. J., and Runnerstrom, E. E., 2002. Coastal uplift of the San Joaquin Hills, southern Los Angeles Basin, California, by a large earthquake since 1635 A.D., *Bulletin of the Seismological Society of America*, v. 92, p. 590-599.

Greene, H. G., and Kennedy, M. P., 1987. Geology of the California continental margin: Explanation of the California continental margin map series, California Division of Mines & Geology, *Bulletin 207*, 110 p.

Hartzell, S. H., aqnd Heaton, T. H., 1983, Inversion of strong ground motion and teleseismic waveform data for the fault rupture history of the 1979 Imperial Valley, California earthquake, *Bulletin of the Seismological Society of America*, v. 73, p. 1553-1583.

Hauksson, Egill, and Jones, L. M., 1988. The July 1986 Oceanside (M_L=5.3) earthquake sequence in the continental borderland, southern California, *Bulletin of the Seismological Society of America*, v. 78, p. 1885-1906.

Hauksson, E., Jones, L. M., and Hutton, K., 1995. The 1994 Northridge earthquake sequence in California: Seismological and tectonic aspects, *Journal of Geophysical Research*, v. 100, p. 12,335-12,355.

Hill, D. P., Eaton, J. P., and Jones, L. M., 1990. Seismicity, 1980-86, chapter 5 in Wallace, R. E. (Editor) The San Andreas Fault System, California: U.S. Geological Survey *Professional Paper 1515*, p. 115-151.

Houston, J. R., 1980. Type 19 flood insurance study, Tsunami predictions for southern California, U.S. Army Corps of Engineers Waterways Experiment Station *Technical Report HL-80-18*, 172 p.

Jacoby, G. C., Sheppard, P. R., and Sieh, K. E., 1988. Irregular recurrence of large earthqukaes along the San Andreas fault, Evidence from trees, *Science*, v. 241, no. 4862, p. 196-199.

Junger, Arne, 1976. Tectonics of the southern California Borderland: *in* Howell, D. G. (Editor) Aspects of the Geological History of the California Continental Borderland: Pacific Section, American Association of Petroleum Geologists, *Miscellaneous Publication 24*, p. 486-498.

Kamerling, Marc, and Luyendyk, B. P., 1979. Tectonic rotations of the Santa Monica Mountains region, western Transverse Ranges, California, suggested by paleomagnetic vectors, *Geological Society of America Bulletin*, v. 90, p. 331-337.

King, G.C.P., Stein, R.S., and Lin, J., 1994. Static stress changes and the triggering of earthquakes, *Bulletin of the Seismological Society of America*, v. 84, p. 935-953.

Lajoie, K. R., Ponti, D. J., Powell II, C. L., Mathieson, S. A., and Sarna-Wojcicki, 1992. Emergent marine strandlines and associated sediments, coastal California: A record of Quaternary sea-level fluctuations, vertical tectonic movements. climatic processes, and coastal processes, in Heath, E. G., and Lewis, W. L., editors, The Regressive Pleistocene Shoreline: Coastal Southern California, South Coast Geological Society Annual Field Trip Guidebook, p. 81-104.

Lander, J. F., Lockridge, P. A., and Kozuch, M. J., 1993. Tsunamis affecting the West Coast of the United States, 1806-1992, US Dept. Commerce, NOAA, *KGRD 29*, Boulder, CO, 242 p.

Larson, K.M., 1993. Application of the Global Positioning System to crustal deformation measurements, 3, Result from the southern California borderlands, *Journal of Geophysical Research*, v. 98, p. 21,713-21,726.

Lee, W. H. K., Yerkes, R. F., and Simirenko, M., 1979. Recent earthquake activity and focal mechanisms in the western Transverse Ranges, California, U. S. Geological Survey *Circular 799-A*, p. 1-26.

Legg, M. R., 1980. Seismicity and tectonics of the inner continental borderland of southern California and northern Baja California, Mexico [M.S. thesis] University of California, Santa Diego, San Diego, California, 60 p.

Legg, M. R., 1985. Geologic Structure and tectonics of the inner continental borderland offshore northern Baja California, Mexico [Ph.D. dissertation] University of California, Santa Barbara, 410 p.

Legg, M. R., 1991. Developments in understanding the tectonic evolution of the California Continental Borderland, *in* Osborne, R.H. (Editor) *From Shoreline to Abyss: F.P. Shepard Commemorative Volume*, SEPM Special Publication 46, p. 291-312.

Legg, M. R., Luyendyk, B. P., Mammerickx, J., de Moustier, C., and Tyce, R. C., 1989. Sea Beam survey of an active strike-slip fault - The San Clemente fault in the California Continental Borderland, *Journal of Geophysical Research*, v. *94*, p. 1727-1744.

Legg, M. R., and Kennedy, M. P., 1991. Oblique divergence and convergence in the California Continental Borderland. *in* Abbott, P.L., and W.J. Elliott (Editors) *Environmental Perils of the San Diego Region*, San Diego Association of Geologists Guidebook, p. 1-16.

Legg, M. R., and Borrero, J. C., 2001. Tsunami potential of major restraining bends along submarine strike-slip faults, in *Proceedings of the International Tsunami Symposium 2001*, NOAA/PMEL, Seattle, WA, p. 331-342.

Legg, M.R., and Kamerling, M.J., 2002. Large-scale basement-involved landslides, California Continental Borderland: in Watts, P., Synolakis, C.E., and Bardet, J.-P., editors, *Prediction of Underwater Landslide Hazards*, Proceedings of the May 2000 Workshop, University of Southern California, *PAGEOPH* (in press).

Legg, M. R., Einstein, D. E., and Wang, H. D., 1999, Deformation history of a major restraining bend along a right-slip fault: the San Clemente fault offshore northern Baja California: SCEC Annual Meeting, Palm Springs, CA, p. 74.

Lindvall, S. C., and Rockwell, T. K., 1995. Holocene activity of the Rose Canyon fault zone in San Diego, California, *Journal of Geophysical Research*, v. 100, p. 24,121-24,132.

Liu, P.L.-F., Synolakis, C.E., and Yeh, H., 1991. Impressions from the First International Workshop on Long Wave Runup, *Journal of Fluid Mechanics, 229*, 675-688.

Luyendyk, B. P., 1991. A model for Neogene crustal rotations, transtension, and transpression in southern California, *Geological Society of America Bulletin*, v. 103, p. 1528-1536.

Magistrale, H., 1993. Seismicity of the Rose Canyon fault zone near San Diego, California, *Bulletin of the Seismological Society of America*, v. 83, p. 1971-1978.

Mann, P. and Gordon, M.B., 1996. Tectonic uplift and exhumation of blueschist belts along transpressional strike-slip fault zones, in Bebout, G. E., Scholl, D.W., Kirby, S.H., and Platt, J.P. (Editors) *Subduction: Top to Bottom*, American Geophysical Union Monograph 96, p. 143-154.

McCarthy, R .J., Bernard, E. N., and Legg, M. R., 1993. The Cape Mendocino earthquake: A local tsunami wakeup call? *Proceedings of the Eighth Symposium on Coastal and Ocean Management*, New Orleans, Louisiana, 19-23 July 1993, p. 2812-2828.

McClay, K., and Bonora, M., 2001. Analog models of restraining stepovers in strike-slip fault systems, *AAPG Bulletin*, v. 85, p. 233-260.

McCulloch, D. S., 1985. Evaluating tsunami potential, in Ziony, J. I., ed., Evaluating earthquake hazards in the Los Angeles Region—An earth science perspective, U.S. Geological Survey *Professional Paper 1360*, p. 375-413.

McNeilan, T.W., Rockwell, T.K., and Resnick, G.S., 1996. Style and rate of Holocene slip, Palos Verdes fault, southern California, *Journal of Geophysical Research*, v. 101, no. B4, p. 8317-8334.

Moore, D. G., 1969. Reflection profiling studies of the California Continental Borderland Structure and Quaternary turbidite basins, Geological Society of America *Special Paper 107*, 142 p.

Morton, D. M., and Matti, J.C., 1993. Extension and contraction within an evolving divergent strike-slip fault complex, The San Andreas and San Jacinto fault zones at their convergence in southern California: in Powell, R.E., Weldon, R.J., II, and Matti, J.C. (Editors) *The San Andreas Fault System: Displacement, palinspastic reconstruction, and geologic evolution*, Boulder, Colorado, Geological Society of America Memoir 178, p. 217-230.

Okada, Y., 1985. Surface deformation due to shear and tensile faults in a half-space, *Bulletin of the Seismological Society of America*, v. 75, p. 1135-1154.

Okada, Y., 1992. Internal deformation due to shear and tensile faults in a half-space, *Bulletin of the Seismological Society of America*, v. 82, p. 1018-1040.

Okal, E., and 11 others, 2001. The Peruvian tsunami of 23 June 2001: Preliminary report by the international tsunami survey team, [abstract] *EOS, Trans. American Geophys. Union,* v. 82, p. F921.

Nardin, T. R., and Henyey, T. L., 1978. Pliocene-Pleistocene diastrophism of the Santa Monica and San Pedro shelves, California Continental Borderland, *AAPG Bulletin*, v. 62, p. 247-272.

Nicholson, Craig, and Crouch, J. K., 1989. Neotectonic structures along the central and southern California margin [abstract]: *Seismological Research Letters*, v. 60, p. 23-24.

NOS, 1999. Hydrographic Survey Data: National Ocean Service, National Oceanic and Atmospheric Administration, National Geophysical Data Center, Boulder, CO, CD-ROM. (updates available via internet).

Plafker, G., and Galloway, J.P., 1989. Lessons Learned from the Loma Prieta, California, Earthquake of October 17, 1989, U.S. Geological Survey *Circular 1045*, 48 p.

Rivero, C., Shaw, J. H., and Mueller, K., 2000. Oceanside and Thirtymile Bank blind thrusts: Implications for earthquake hazards in coastal southern California, *Geology*, v. 28, p. 891-894.

Rockwell, T.K., Lindvall, S., Herzberg, M., Murbach, D., Dawson, T., and Berger, G., 2000. Paleoseismology of the Johnson Valley, Kickapoo, and Homestead Valley faults: Clustering of earthquakes in the Eastern California Shear Zone, *Bulletin of the Seismological Society of America*, v. 90, p. 1200-1236.

Satake, K., and Somerville, P. G., 1992. Location and size of the 1927 Lompoc, California, earthquake from tsunami data, *Bulletin of the Seismological Society of America*, v. 82, p. 1710-1725.

Schwing, F.B., Norton, J.G., and Pilskaln, C.H., 1990. Earthquake and Bay: Response of Monterey Bay to Loma Prieta Earthquake, *EOS, Trans. American Geophysical Union*, v. 71, p. 250-252.

Seeber, L., and Armbruster, J. G., 1995. The San Andreas fault system through the Transverse Ranges as illuminated by earthquakes, *Journal of Geophysical Research*, v. 100, p. 8285-8310.

Sella, G. F., Dixon, T. H., and Mao, A., 2002. REVEL: A model for Recent plate velocities from space geodesy, *Journal of Geophysical Research*, v. 107, p. ETG 11-1 to 11-31.

Sharp, R. V., 1982. Comparison of 1979 surface faulting with earlier displacements in the Imperial Valley, in *The Imperial Valley, California, Earthquake of October 15, 1979*, U.S. Geological Survey *Professional Paper 1254*, p. 213-222.

Shepard, F. P., and Emery, K. O., 1941. Submarine topography off the southern California coast: Canyons and tectonic interpretation, Geological Society of America *Special Paper 31*, 171 p.

Shepard, F. P., Grant, U. S., IV, and Dietz, R. S., 1939. The emergence of Santa Catalina Island, *American Journal of Science*, v. 237, p. 651-655.

Sibson, R. H., 1982. Fault zone models, heat flow, and the depth distribution of earthquakes in the continental crust of the United States, *Bulletin of the Seismological Society of America*, v. 72, p. 151-164.

Sibson, R. H., 1985. Stopping of fault ruptures at dilational fault jogs, *Nature*, v. 316, p. 248-251.

Sieh, K. E., Stuiver, M., and Brillenger, D., 1989. A more precise chronology of earthquakes produced by the San Andreas fault in southern California, *Journal of Geophysical Research*, v. 94, p. 603-623.

Sieh, K., Jones, L., Hauksson, E., Hudnut, K., Eberhart-Phillips, D., Heaton, T., Hough, S., Hutton, K., Kanamori, H., Lilje, A., Lindvall, S. McGill, S., Mori, J., Rubin, C. Spotila, J., Stock, J., Thio, H.K., Treiman, J., Wernicke, B., and Zachariasen, J., 1993. Near-field investigations of the Landers earthquake sequence, April to July, 1992, *Science*, v. 260, 171-176.

Sylvester, A. G., 1988. Strike-slip faults, *Geological Society of America Bulletin*, v. 100. p. 1666-1703.

Synolakis, C. E., Bardet, J-P., Borrero, J. C., Davies, H. L., Okal, E. A., Silver, E. A., Sweet, S., and Tappin, D. R., 2002. The slump origin of the 1998 Papua New Guinea Tsunami, *Proc. R. Soc.*

London, A v. 458, p. 763-789.

ten Brink, U. S., Zhang, J., Brocher, T. M., Okaya, D. A., Klitgord, K. D., & Fuis, G. S., 2000. Geophysical evidence for the evolution of the California Inner Continental Borderland as a metamorphic core complex, *Journal of Geophysical Research*, v. 105, p. 5835-5857.

Titov, V., and Synolakis, C., 1995. Modeling of breaking and non-breaking long-wave evolution and runup using VTCS-2, *Journal of Waterway, Port, Coastal and Ocean Engineering*, Nov./Dec., 308-316.

Titov, V., and Gonzáles, F., 1997. Implementation and testing of the method of splitting tsunami (MOST) model, *NOAA Technical Memorandum ERL PMEL-112*.

Toda, S., Stein, R.S., Reasenberg, P.A., and Dieterich, J.H., 1998. Stress transferred by the M_w=6.5 Kobe, Japan, shock: Effect on aftershocks and future earthquake probabilities, *Journal of Geophysical Research*, v. 103, p. 24,543-24,565.

Treiman, J. A, Kendrick, K. J., Bryant, W. A., Rockwell, R. K., and McGill, S. F., 2002. Primary surface rupture associated with the M_W 7.1 16 October 1999 Hector Mine earthquake, San Bernardino County, California, *Bulletin of the Seismological Society of America*, v. 92, p. 1171-1191.

Tucker, A. Z., and Dolan, J. R., 2001. Paleoseismologic evidence for a >8 ka age of the most recent rupture on the eastern Sierra Madre fault, northern Los Angeles metropolitan region, California, *Bulletin of the Seismological Society of America*, v. 91, p. 232-249.

USGS, 1982. *The Imperial Valley, California, Earthquake of October 15, 1979*, U.S. Geological Survey *Professional Paper 1254*, 451 p.

Valensise, G., and Ward, S.N., 1990. Long-term uplift of the Santa Cruz coastline in response to repeated earthquakes along the San Andreas fault, *Bulletin of the Seismological Society of America*, v. 81, p. 1694-1704.

Vedder, J. G., 1987. Regional geology and petroleum potential of the southern California borderland. in *Geology and resource potential of the continental margin of western North America and adjacent ocean basins, Beaufort Sea to Baja California*, Scholl, D. W., Grantz, A., and Vedder, J.G. (Editors) Circum-Pacific Council for Energy and Mineral Resources, Houston, Texas, Earth Science Series, 6, 403-447.

Vedder, J. G., Beyer, L. A., Junger, Arne, Moore, G. W., Roberts, A. E., Taylor, J. C., and Wagner, H. C., 1974. Preliminary report on the geology of the Continental Borderland of southern California, U.S. Geological Survey, Miscellaneous Field Studies *Map MF-624*, Scale 1:500,000.

Vedder, J. G., Howell, D. G., and Forman, J. A., 1979. Miocene strata and their relation to other rocks Santa Catalina Island, California, *in* Armentrout, J. M., Cole, M. R., and TerBest, H., Jr. (Editors) *Cenozoic paleogeography of the western United States,* Society of Economic Paleontologists and Mineralogists, Pacific Coast Paleogeography Symposium 3, p. 239-256.

Vedder, J. G., Greene, H. G., Clarke, S. H., and Kennedy, M. P., 1986. Geologic map of the mid-southern California continental margin, California Division of Mines and Geology, *California Continental Margin Geologic Map Series*, Area 2 of 7, sheet 1 of 4, scale 1:250,000.

Wald, D. J., and Heaton, T. H., 1994. Spatial and temporal distribution of slip for the 1992 Landers, California, earthquake, *Bulletin of the Seismological Society of America*, v. 84, p. 668-691.

Ward, S.N., and Valensise, G., 1994. The Palos Verdes terraces, California: Bathtub rings from a buried reverse fault, *Journal of Geophysical Research*, v. 99, no. B3, p. 4485-4494.

Weldon, R. J., II, Meisling, K. E., and Alexander, J., 1993. A speculative history of the San Andreas fault in the Central Transverse Ranges, California, in Powell, R.E., Weldon, R.J., II, and Matti, J.C. (Editors) *The San Andreas Fault System: Displacement, palinspastic reconstruction, and geologic evolution*, Boulder, Colorado, Geological Society of America Memoir 178, p. 161-198.

Wells, D., and Coppersmith, K., 1994. New empirical relationships among magnitude, rupture length, rupture width, rupture area, and surface displacement, *Bulletin of the Seismological Society of America*, v. 84, p. 974-1002.

White, B. C., 1991. Right-lateral faulting of Santa Catalina Island, California: [Senior Thesis], Department of Geological Sciences, San Diego State University, 30 p.

Wilcox, R. E., Harding, T. P., and Seeley, D. R., 1973. Basic wrench tectonics, *AAPG Bulletin*, v. 57, p. 74-96.

EVALUATION OF TSUNAMI RISK TO SOUTHERN CALIFORNIA COASTAL CITIES

APPENDICES

Appendix A - Figures

Figure 1.Map showing major faults of the southern California region. Northwest-trending faults are right-slip in character. The “big bend” of the San Andreas fault curves from the Salton Trough to the Great Valley. Major offshore faults include the Newport-Inglewood-Rose Canyon (NIRC), Palos Verdes - Coronado Bank (PVCB), San Diego Trough, and San Clemente. (Shaded relief base map from NOAA State DEM).

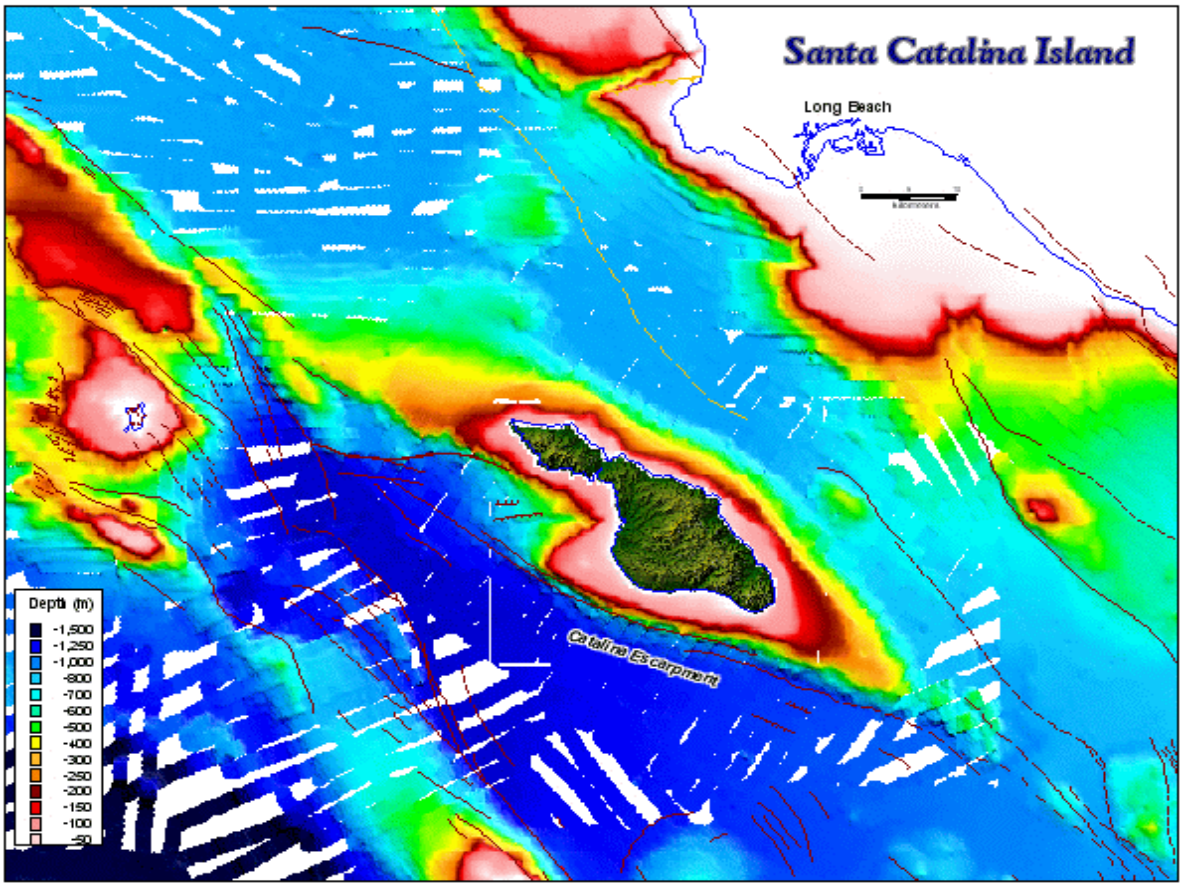

Figure 2. Map showing bathymetry and faulting in the vicinity of Santa Catalina Island. The uplift of the island and surrounding seafloor results from the restraining bend (left bend) along the right-lateral San Diego Trough, Catalina Escarpment, and Santa Cruz - Catalina Ridge fault zone. Shaded relief for island is from USGS DEM; bathymetry from NOAA hydrographic data (1999).

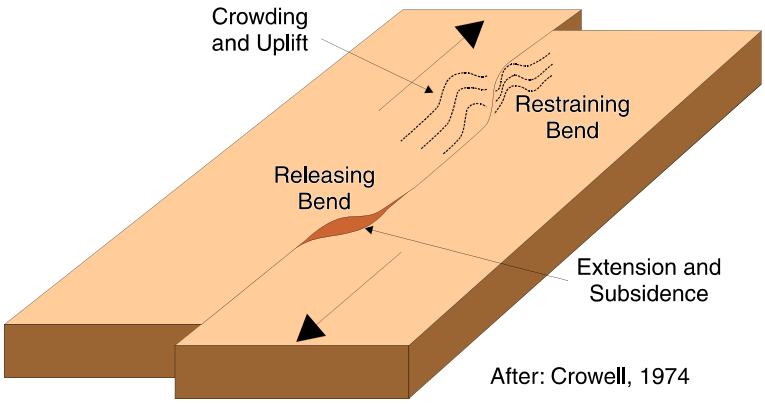

Figure 3. Material crowded into a restraining bend along a strike-slip fault results in convergence, folding and reverse faulting that creates a local uplift. In contrast, extension and subsidence occurs at a releasing bend.

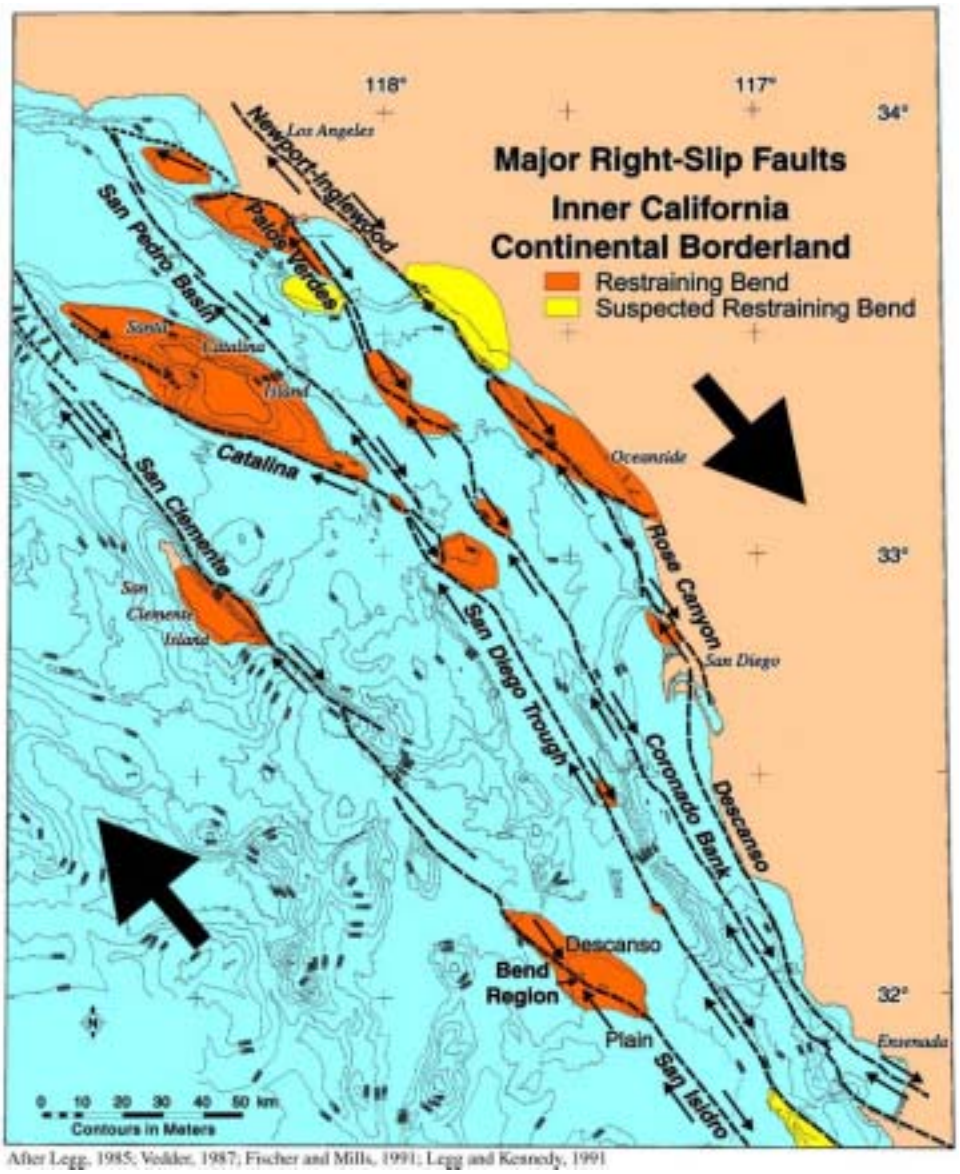

After Legg, 1985; Vedder, 1987; Fischer and Mills, 1991; Legg and Kennedy, 1991

Figure 4. Active strike-slip faults of the Inner California Continental Borderland have sinuous traces with many restraining and releasing bends. The major restraining bend along the San Diego Trough fault system represented by the Santa Catalina Island uplift is the focus of this study.

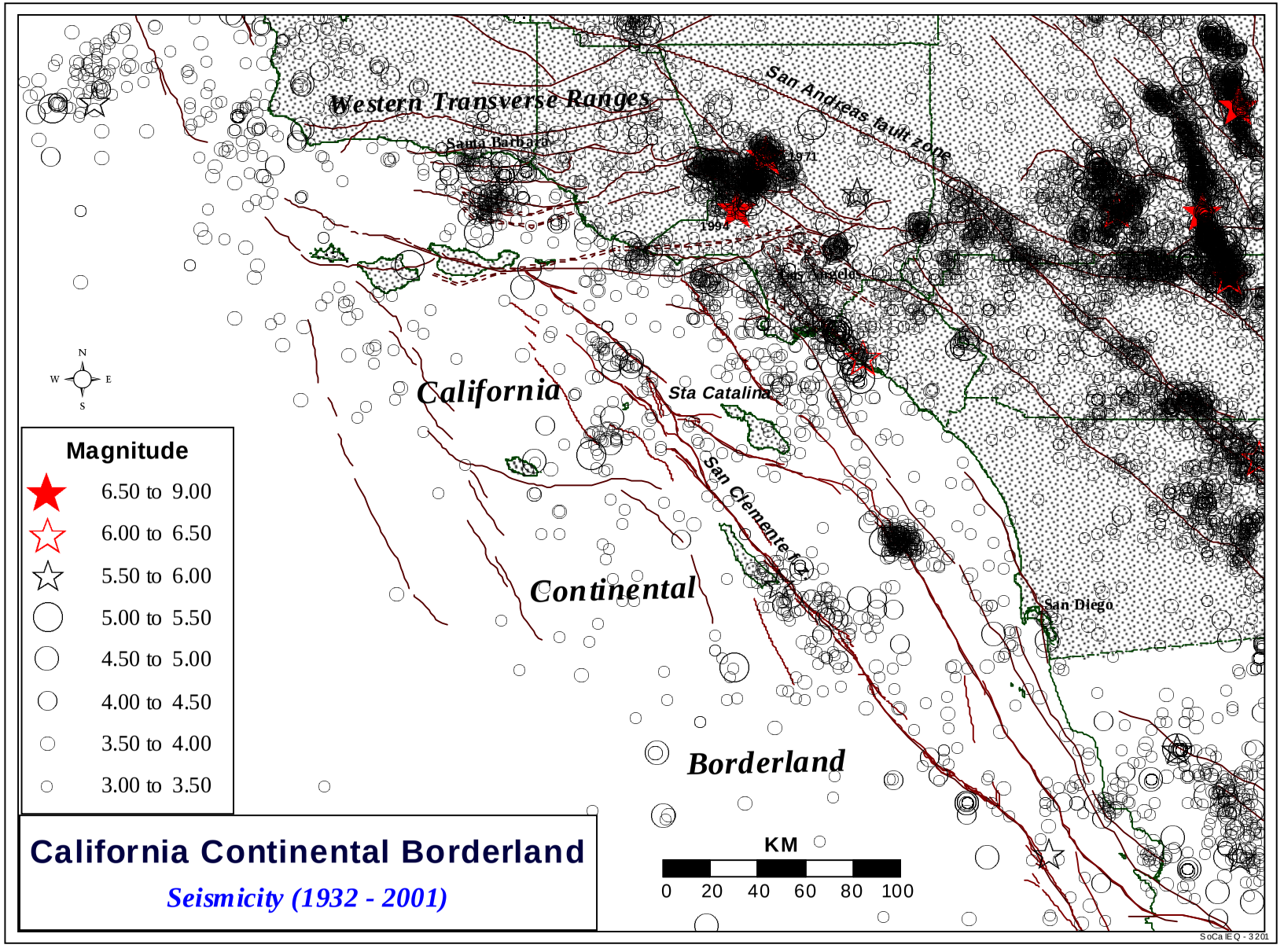

Figure 5. Map showing seismicity of coastal and offshore southern California (data from the Southern California Seismograph Network).

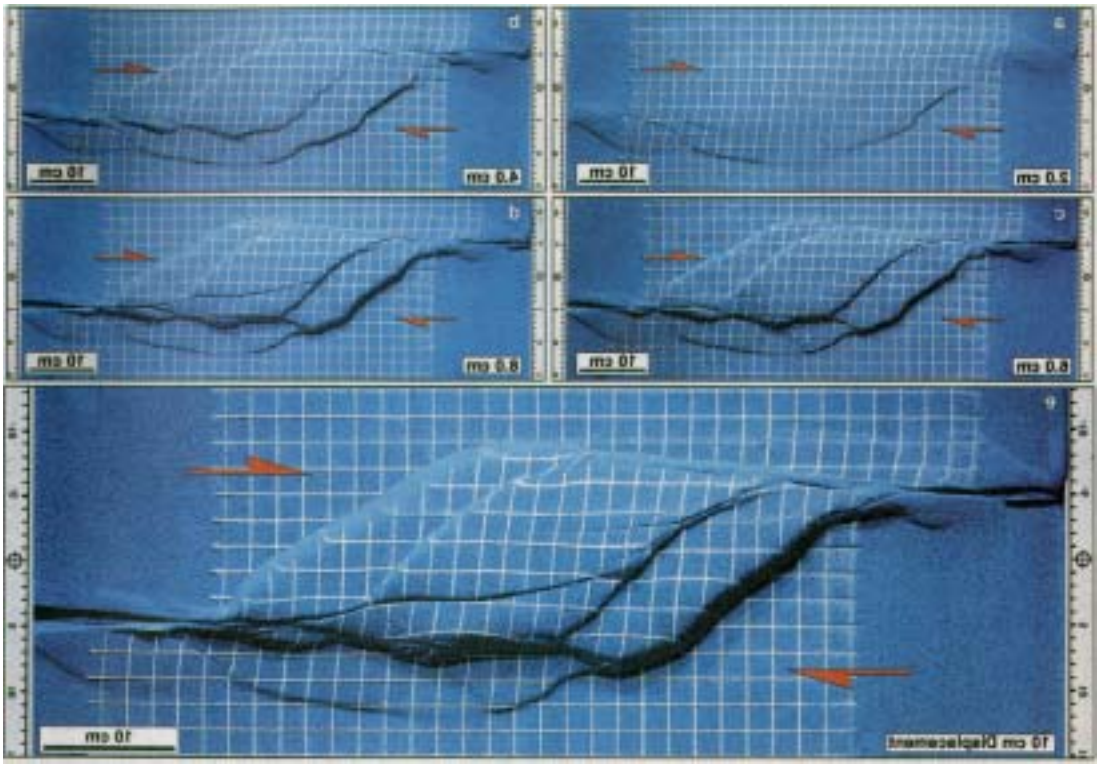

Figure 6a. Analog Model of Restraining Bend Pop-Up Structure
Flipped for right slip (after McClay and Bonora,2001)

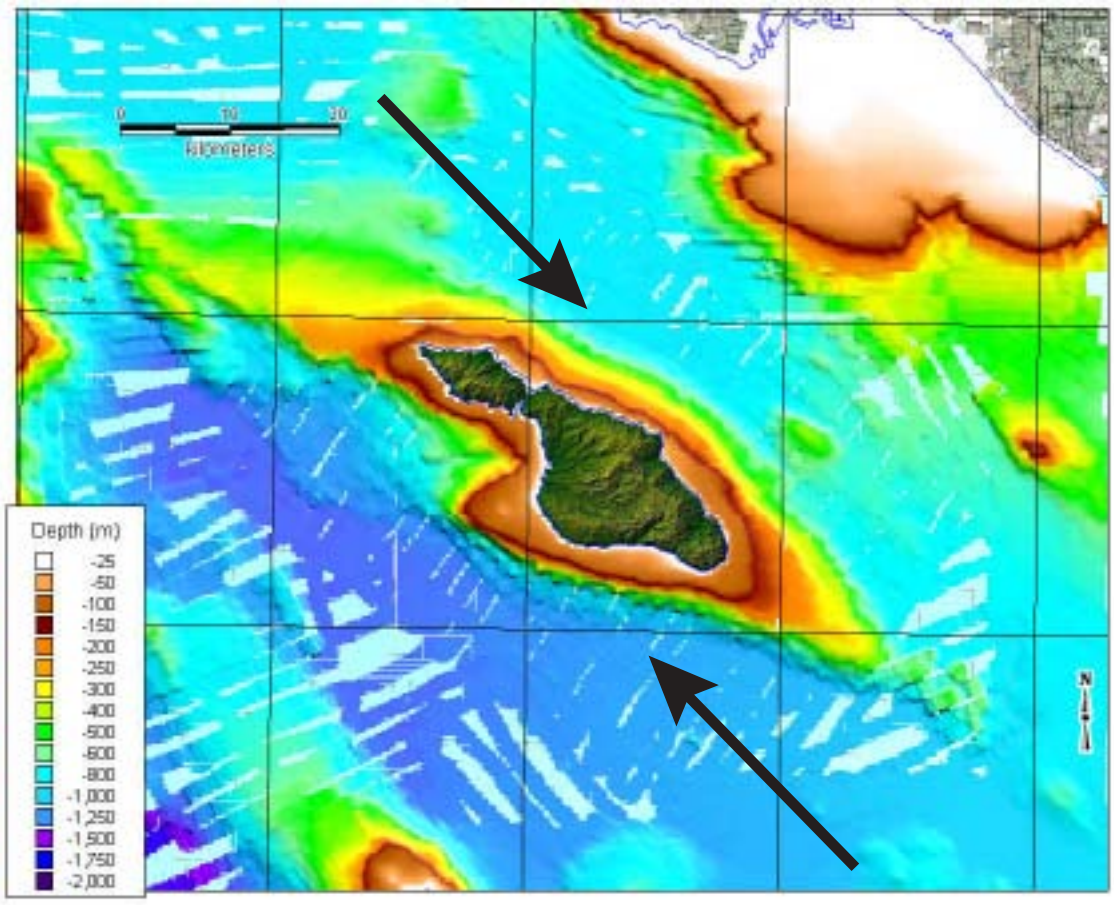

Figure 6b. Shaded Relief Map for the Santa Catalina Island Restraining Bend Pop-Up. Note the Rhomboid Shape. Arrows show inferred direction of right-slip.

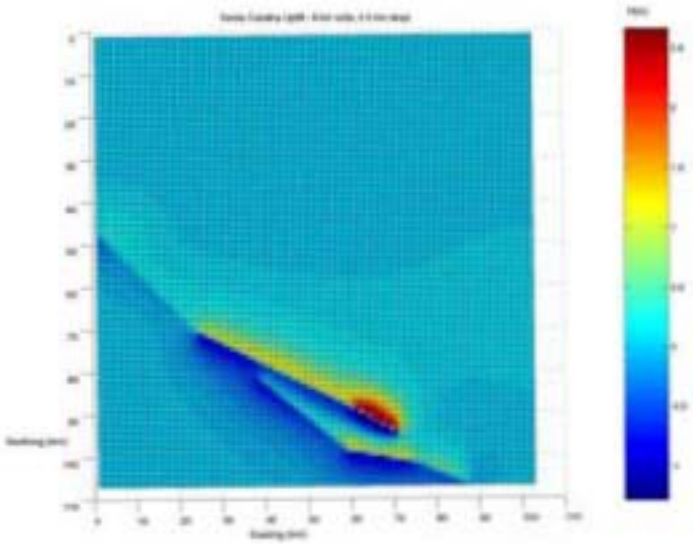

a) Narrow fault (8 km) and shallow depth (0.5 km) produces narrow seafloor uplift and initial wave.

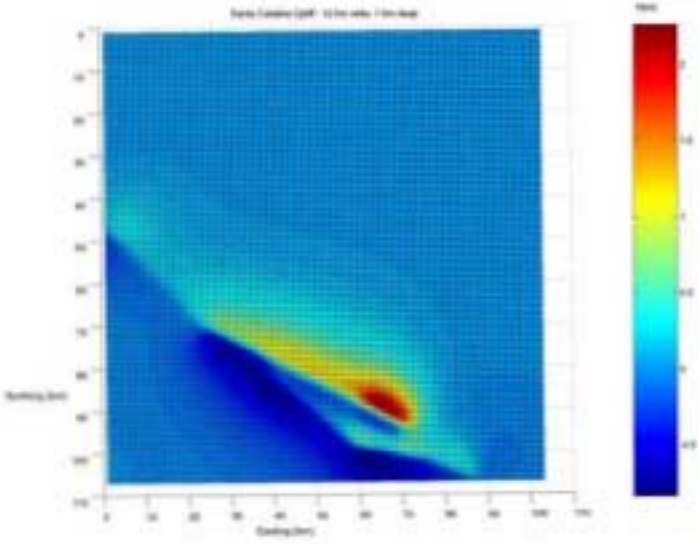

b) Wide fault (12 km) but shallow depth (1 km) produces better fit to island, but still too narrow.

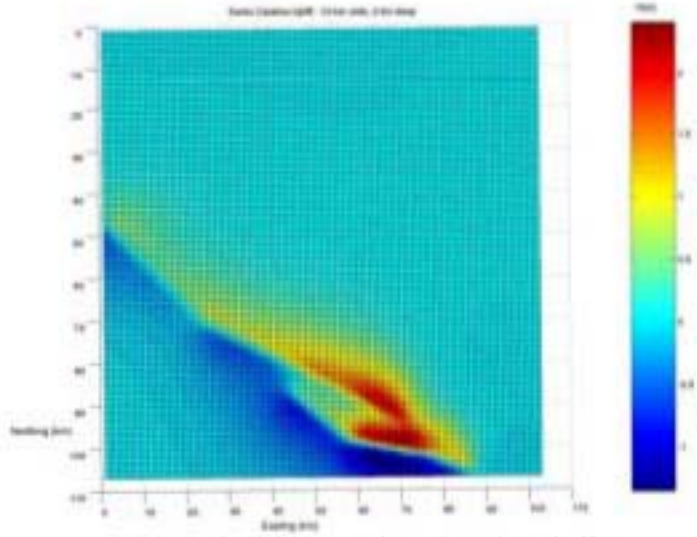

c) Wide fault (14 km) and moderate to shallow depth (2 km) produces uplift that matches island.

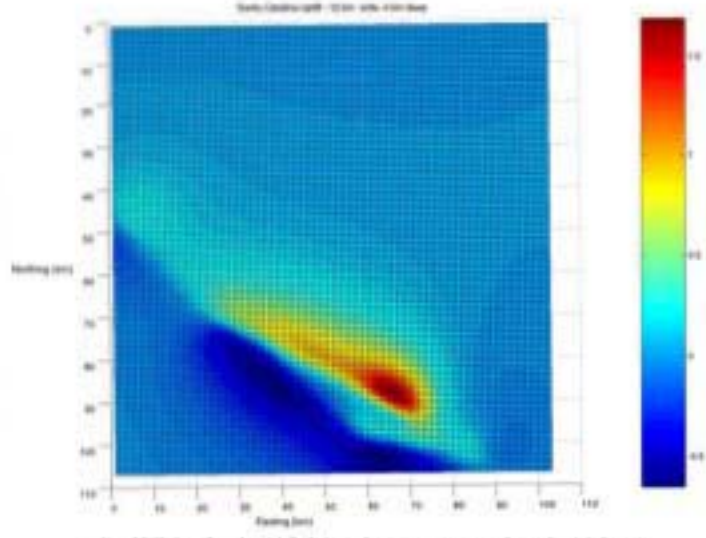

d) Wide fault (12 km) but greater depth (4 km) produces uplift that is too broad.

Figure 7. Elastic dislocation models of the surface uplift predicted using seven planar, rectangular, segments along the Catalina fault showing the variation with regard to fault width and subsurface depth.

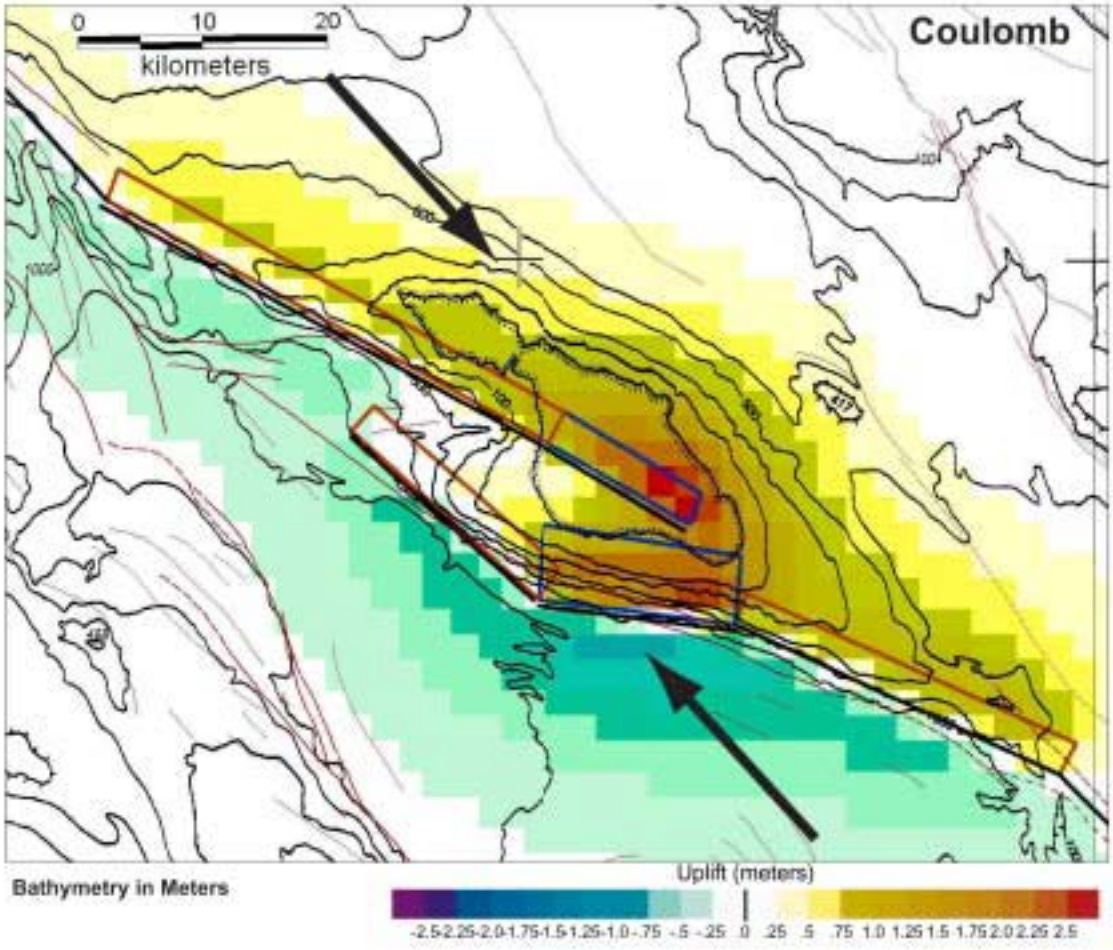

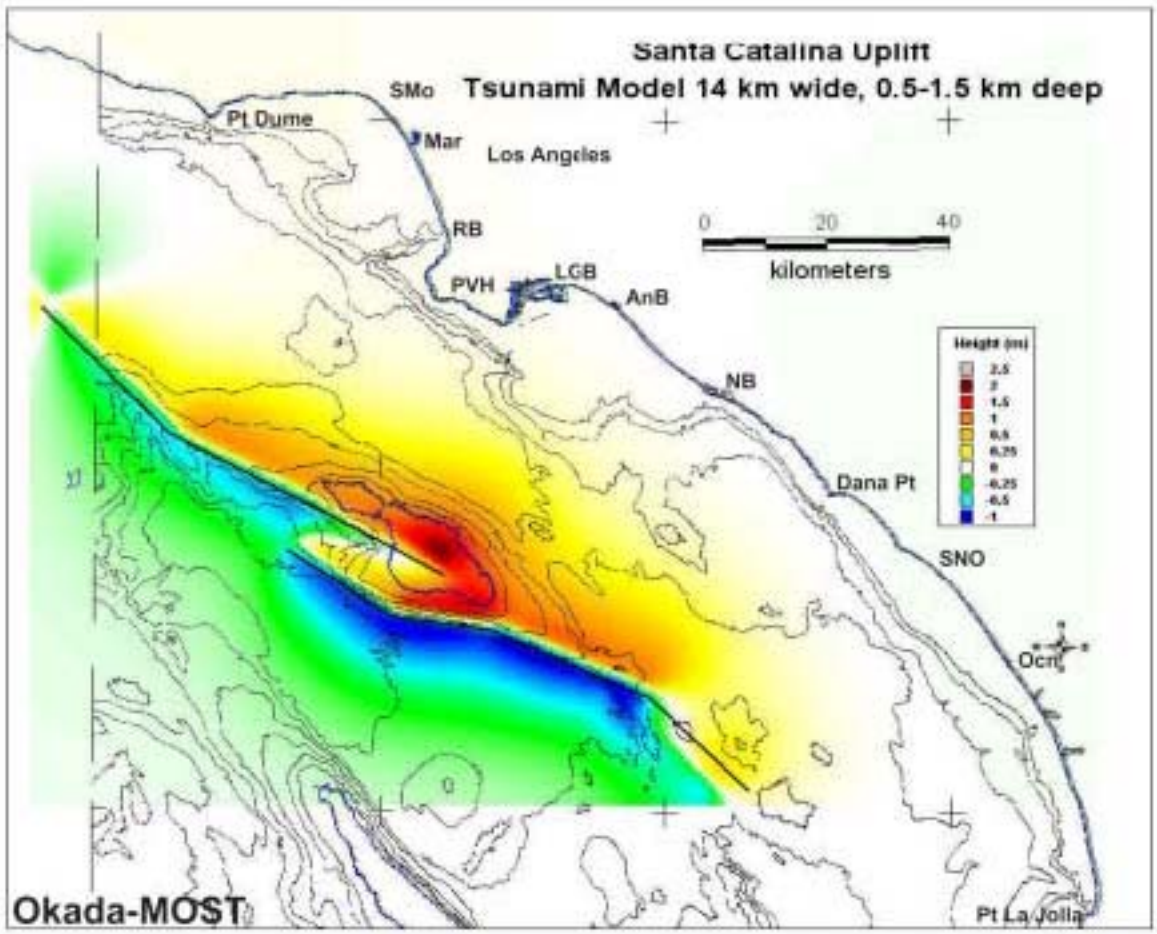

Figure 8. Map comparing uplift produced by elastic dislocation model with 7 segment Catalina fault using the Coulomb program (top) and the initial sea surface uplift condition using the Okada dislocation model for the MOST program (Bottom). Final fault parameters are shown in Table 2. Uplift matches bathymetry contours.

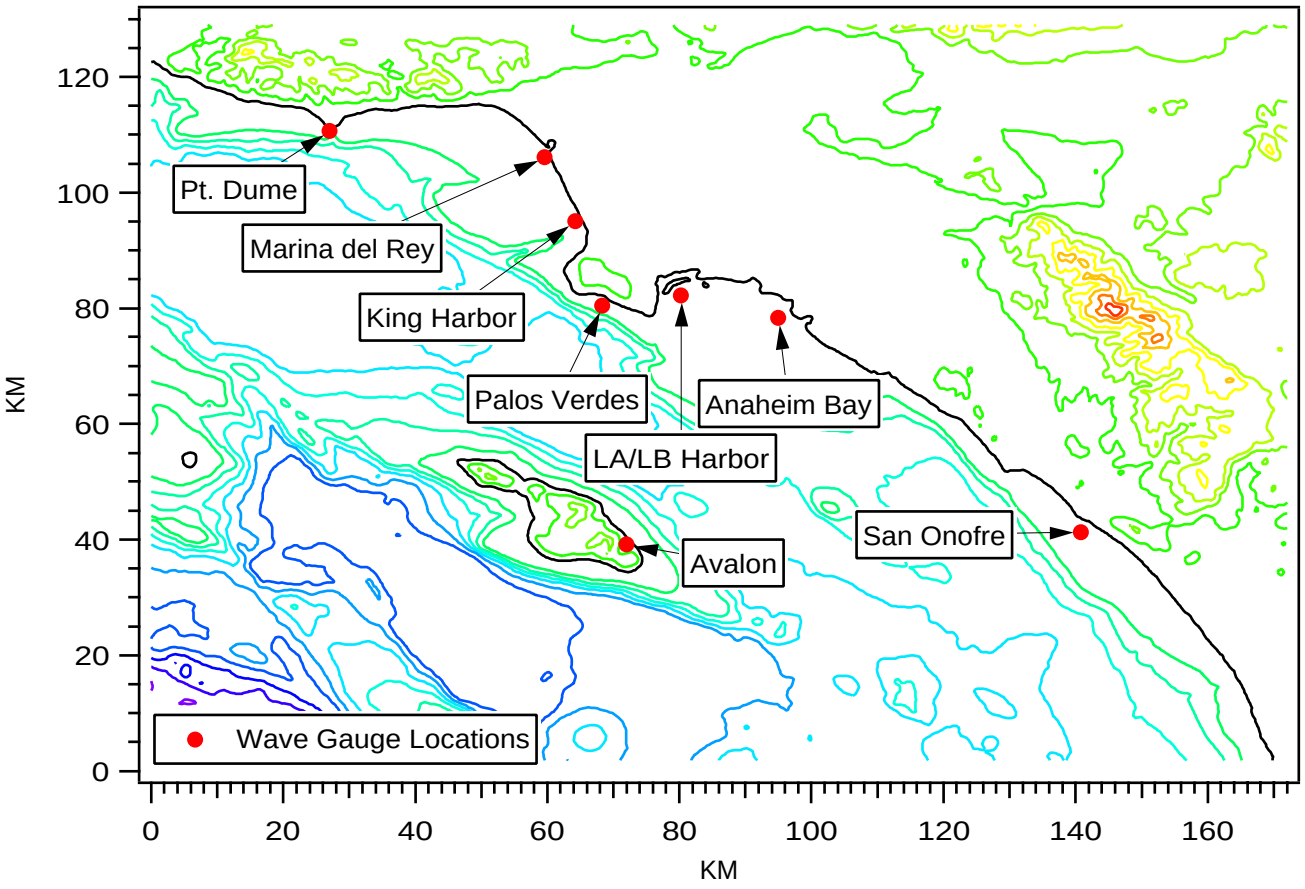

Figure 9. Map showing the extent of the bathymetry/topography grid where the MOST tsunami propagation calculations were performed. Wave gauge locations are plotted and wave gauge parameters are listed in Table 3.

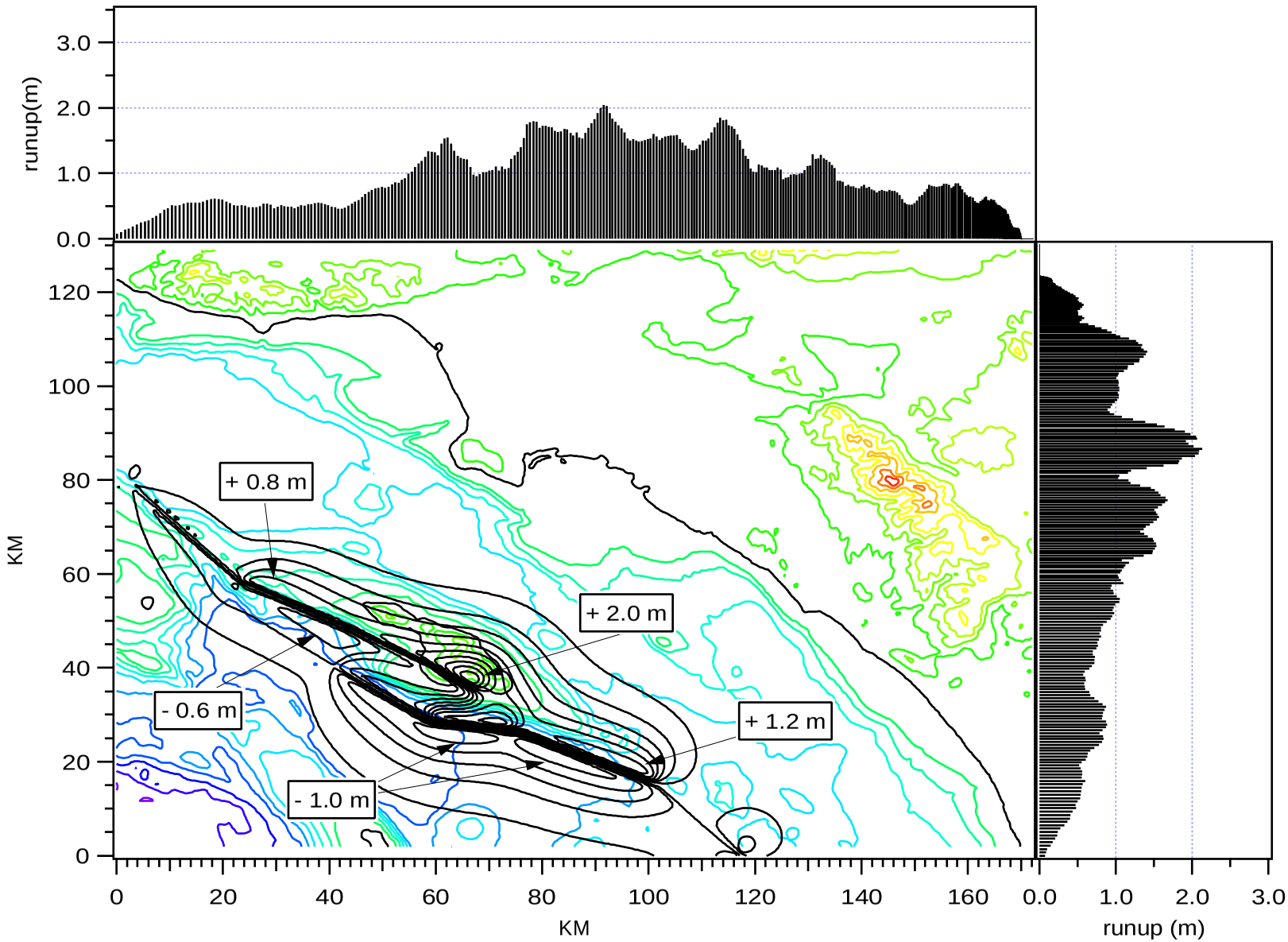

Figure 10. Map showing initial wave height for the full seven segment Catalina fault model with graphs of run-up along the south-facing and west-facing shorelines.

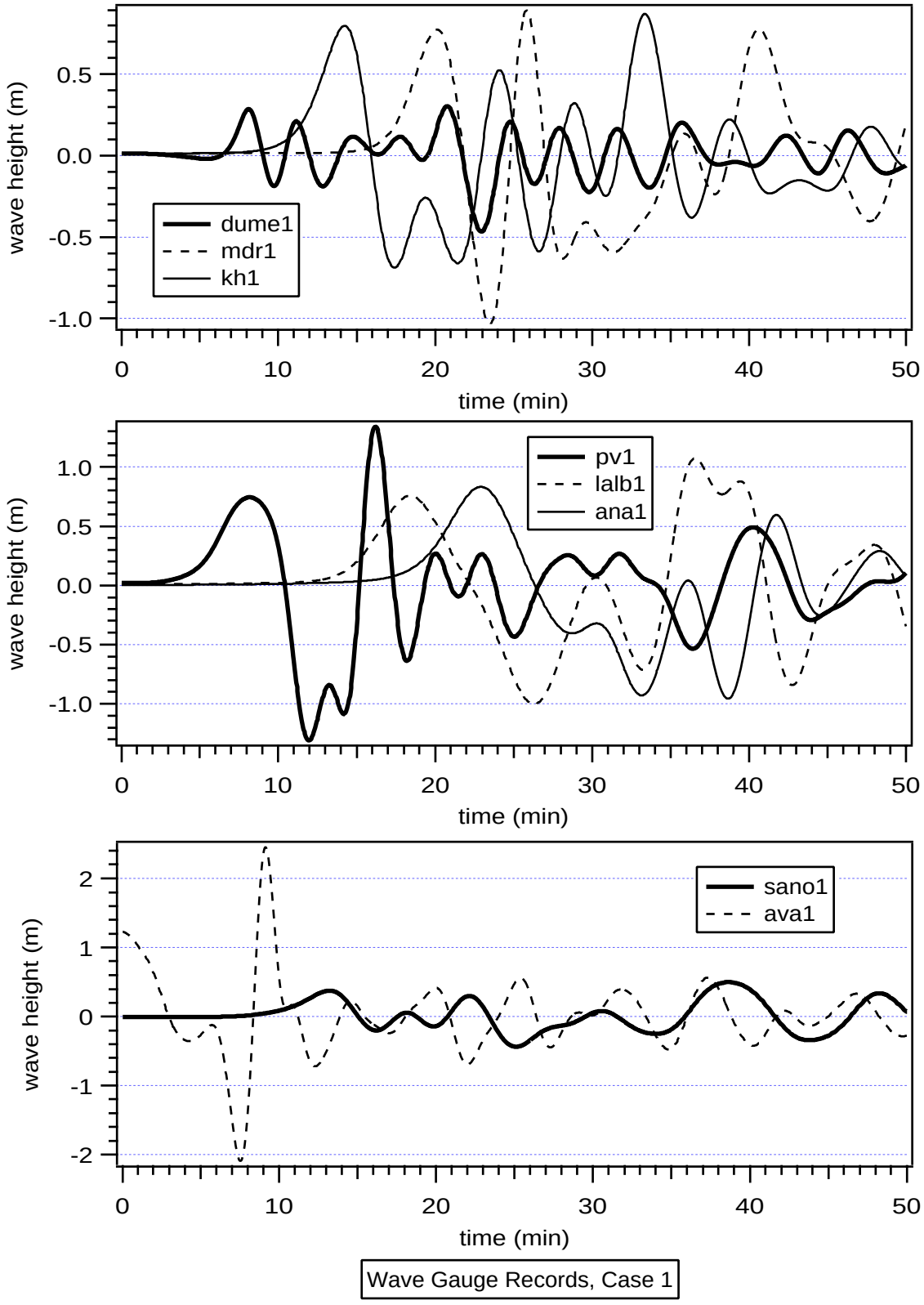

Figure 11. Wave gauge records for the full 7-segment Catalina fault (M=7.7) earthquake (Case 1).

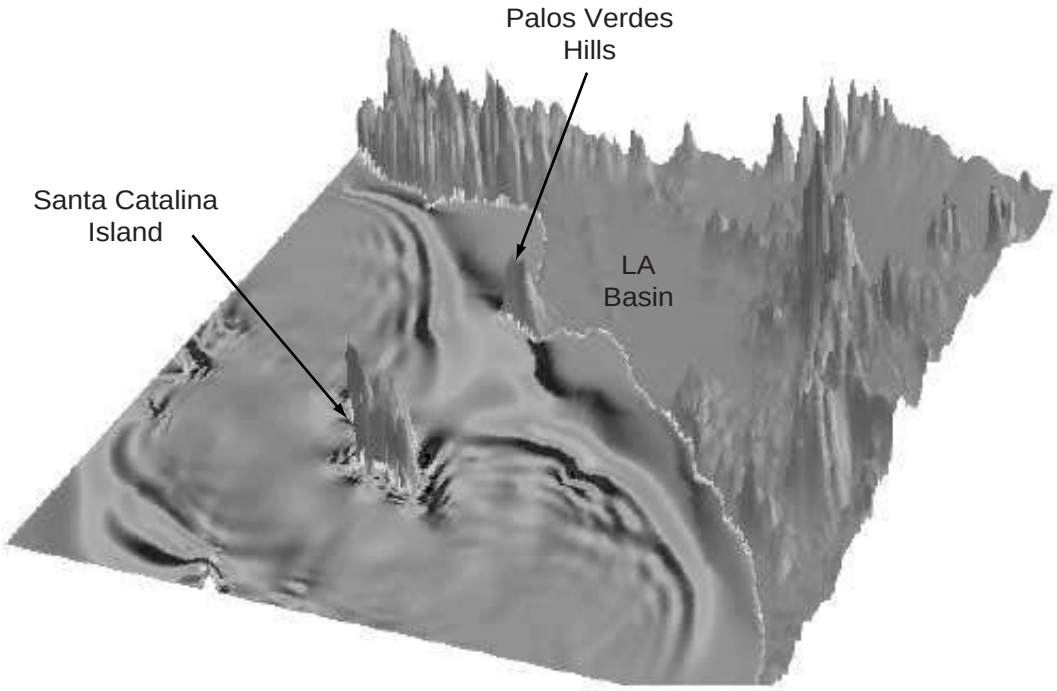

Figure 12. Time step in the MOST tsunami propagation simulation showing the two principal wave fronts generated from the northwest end and southeast end of the submerged Santa Catalina Island platform. Topography has large vertical exaggeration.

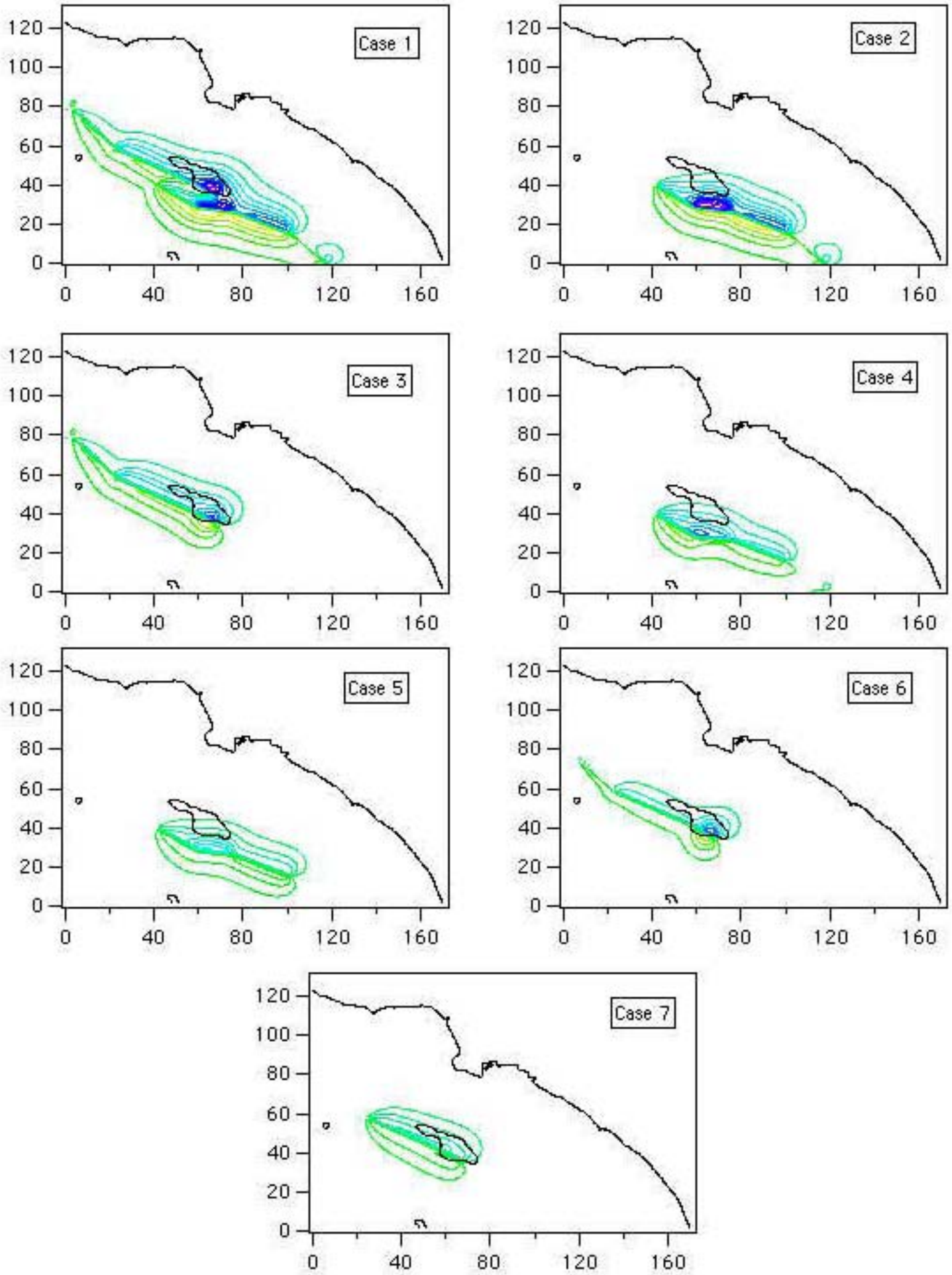

Figure 13. Maps of the initial wave height conditions for the seven Catalina fault tsunami scenarios (Table 4).

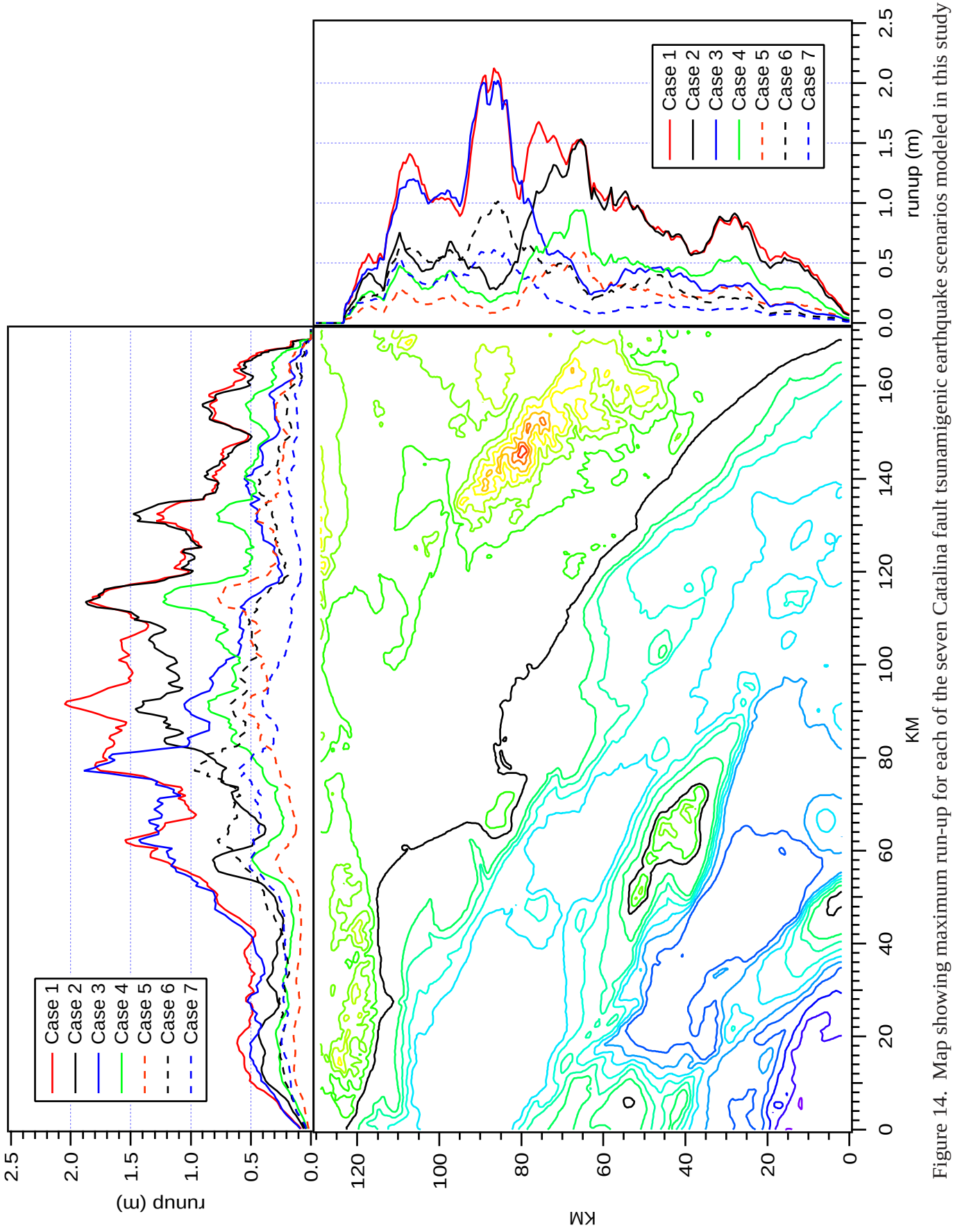

Figure 14. Map showing maximum run-up for each of the seven Catalina fault tsunamigenic earthquake scenarios modeled in this study (see Table 4 for fault parameters).

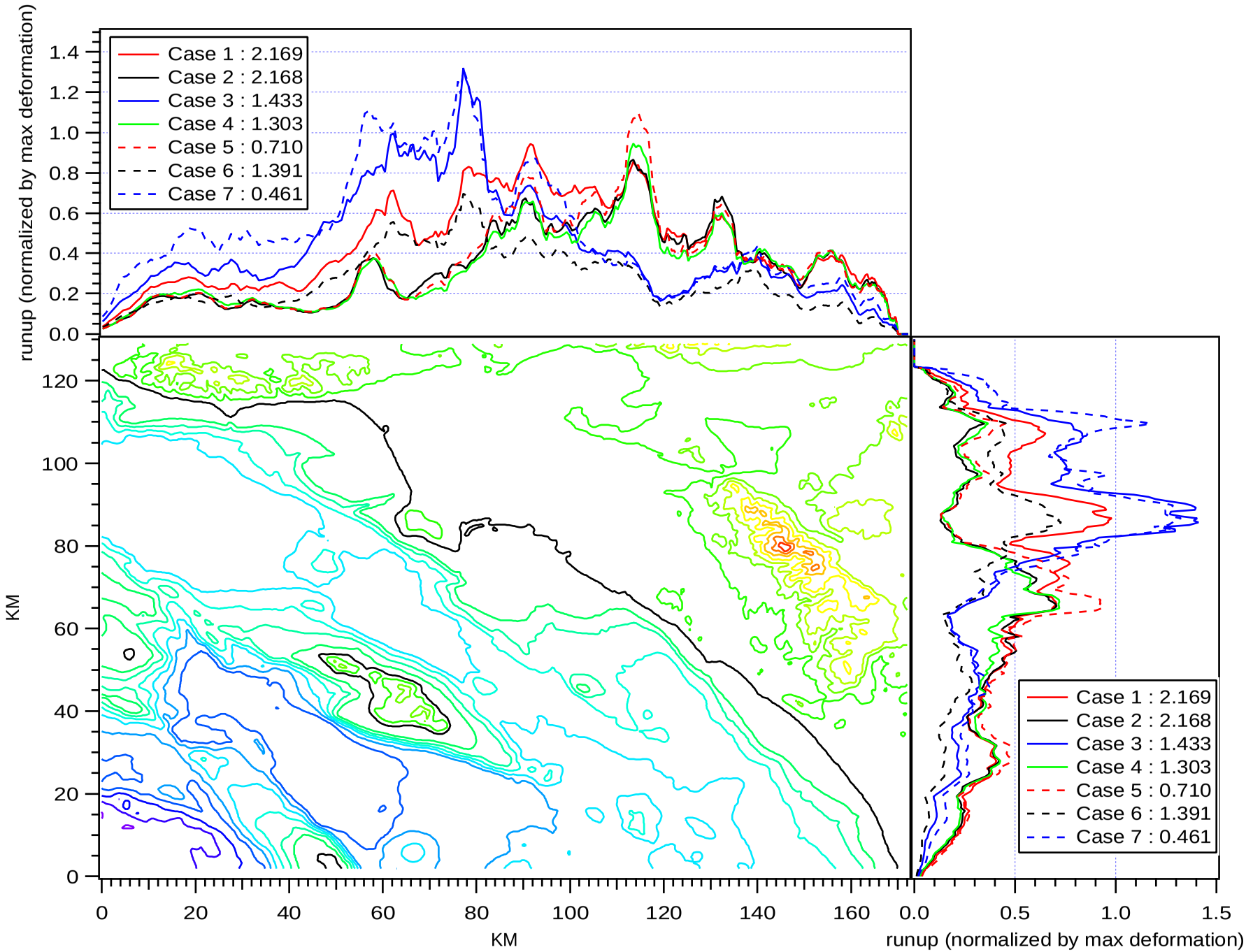

Figure 15. Plot showing maximum run-up for each of the seven Catalina fault tsunamigenic earthquake scenarios modeled in this study (see Table 4 for fault parameters).

EVALUATION OF TSUNAMI RISK FOR COASTAL SOUTHERN CALIFORNIA CITIES

APPENDIX B

Wave Gauges for Cases 2-7

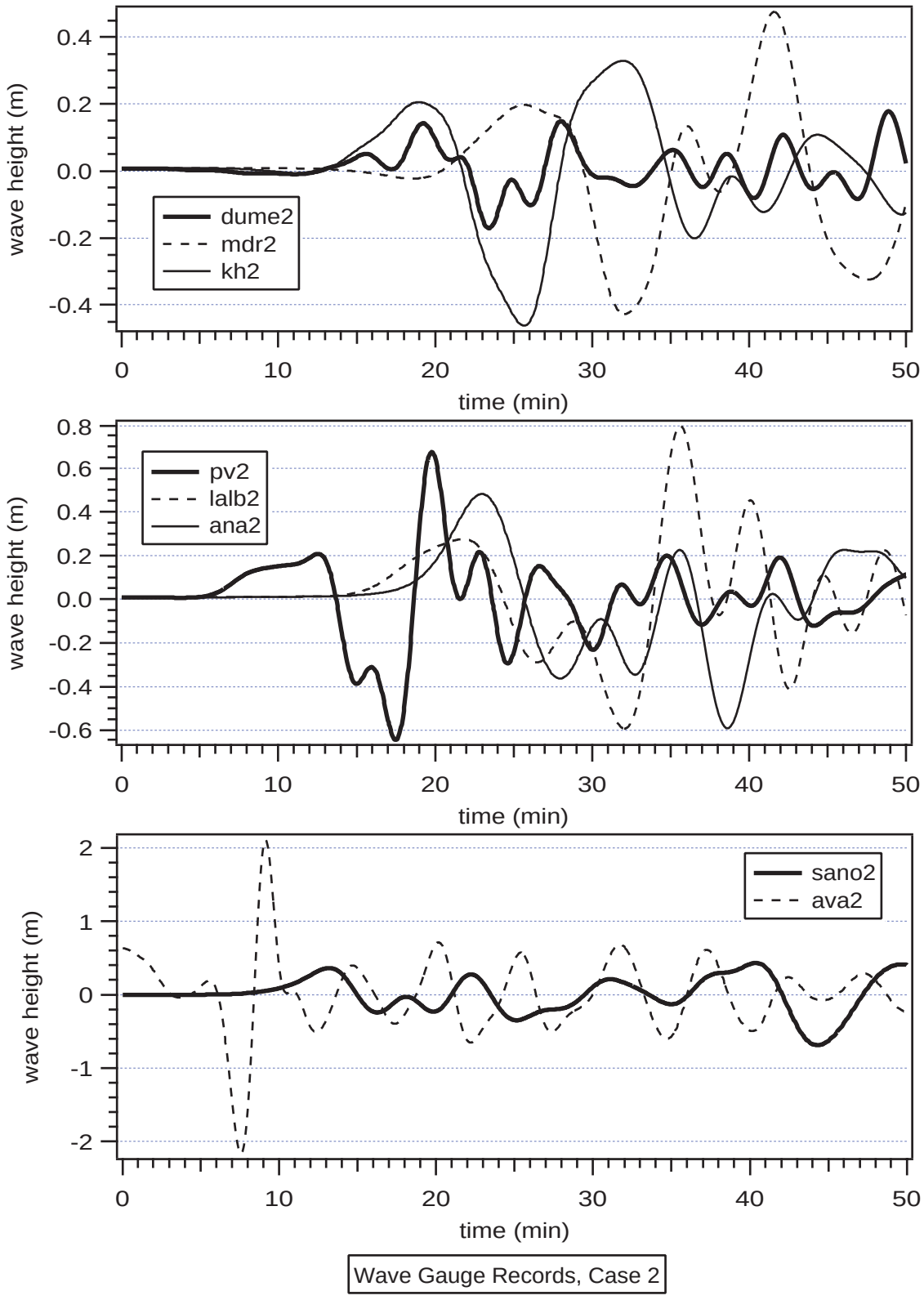

Figure 1. Wave gauge records for segments 1 through 4 of the Catalina fault (M=7.4) earthquake (Case 2).

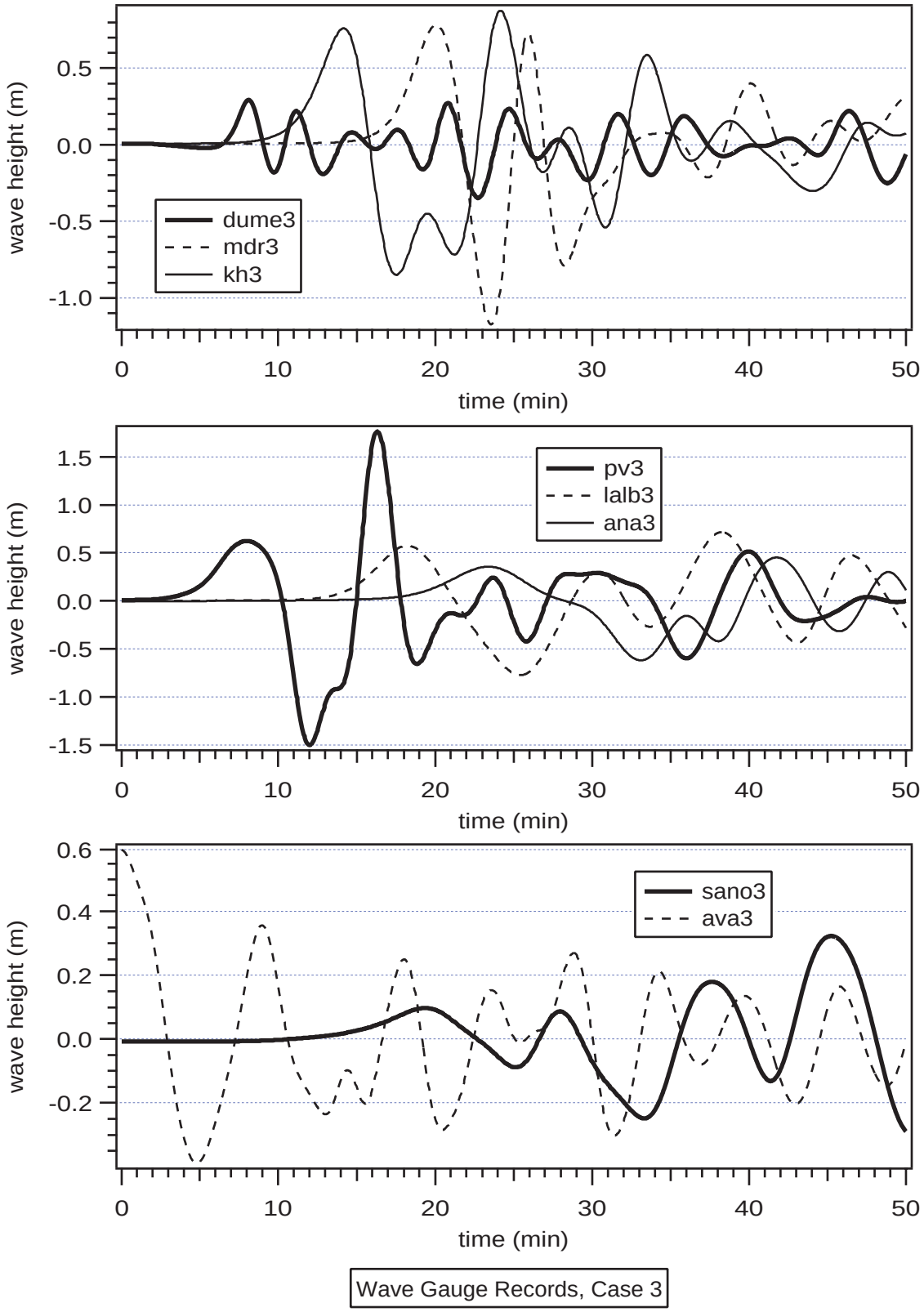

Figure 2. Wave gauge records for segments 5 through 7 of the Catalina fault (M=7.4) earthquake (Case 3).

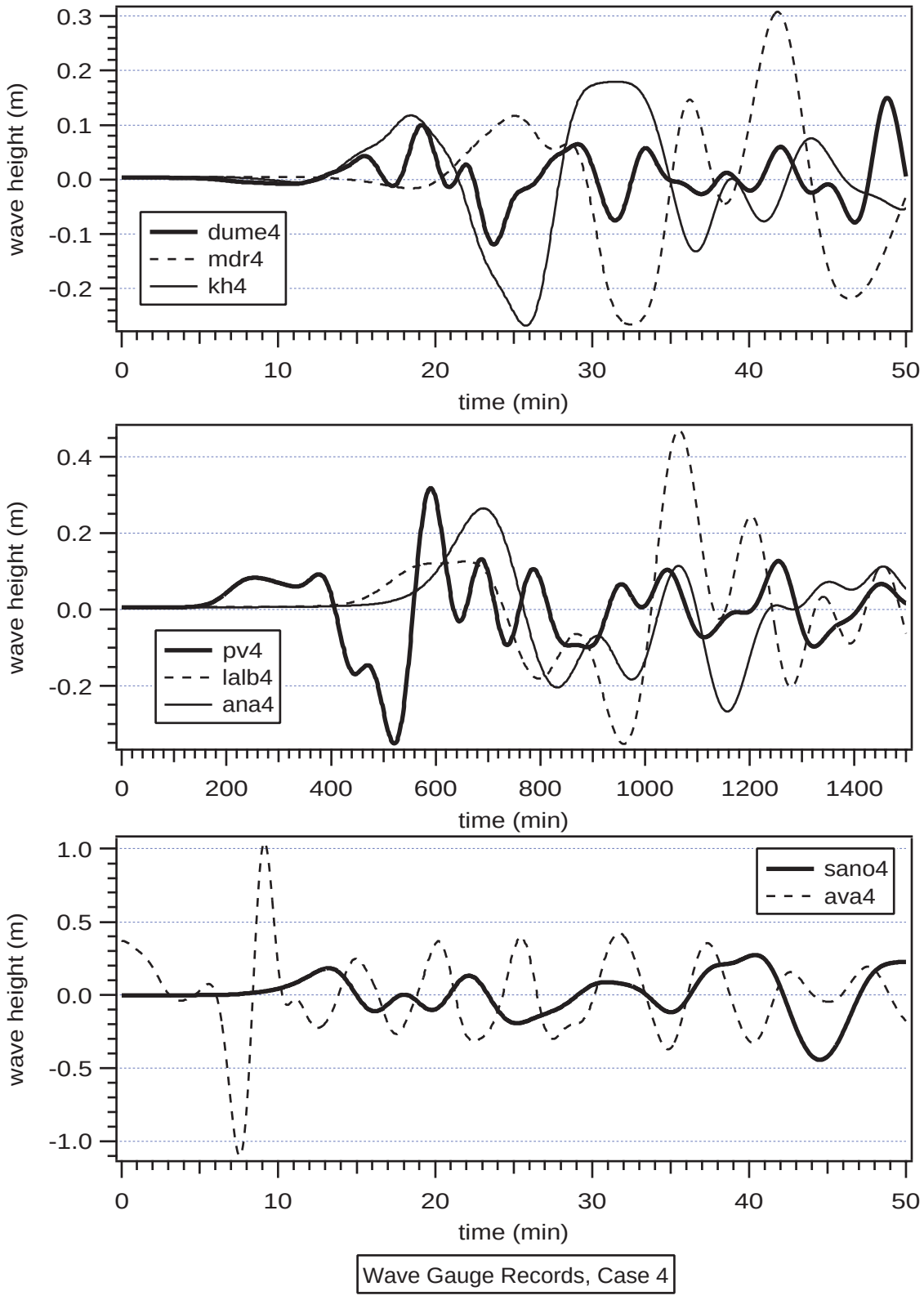

Figure 3. Wave gauge records for segments 1 through 4 of the Catalina fault (M=7.3) earthquake (Case 4).

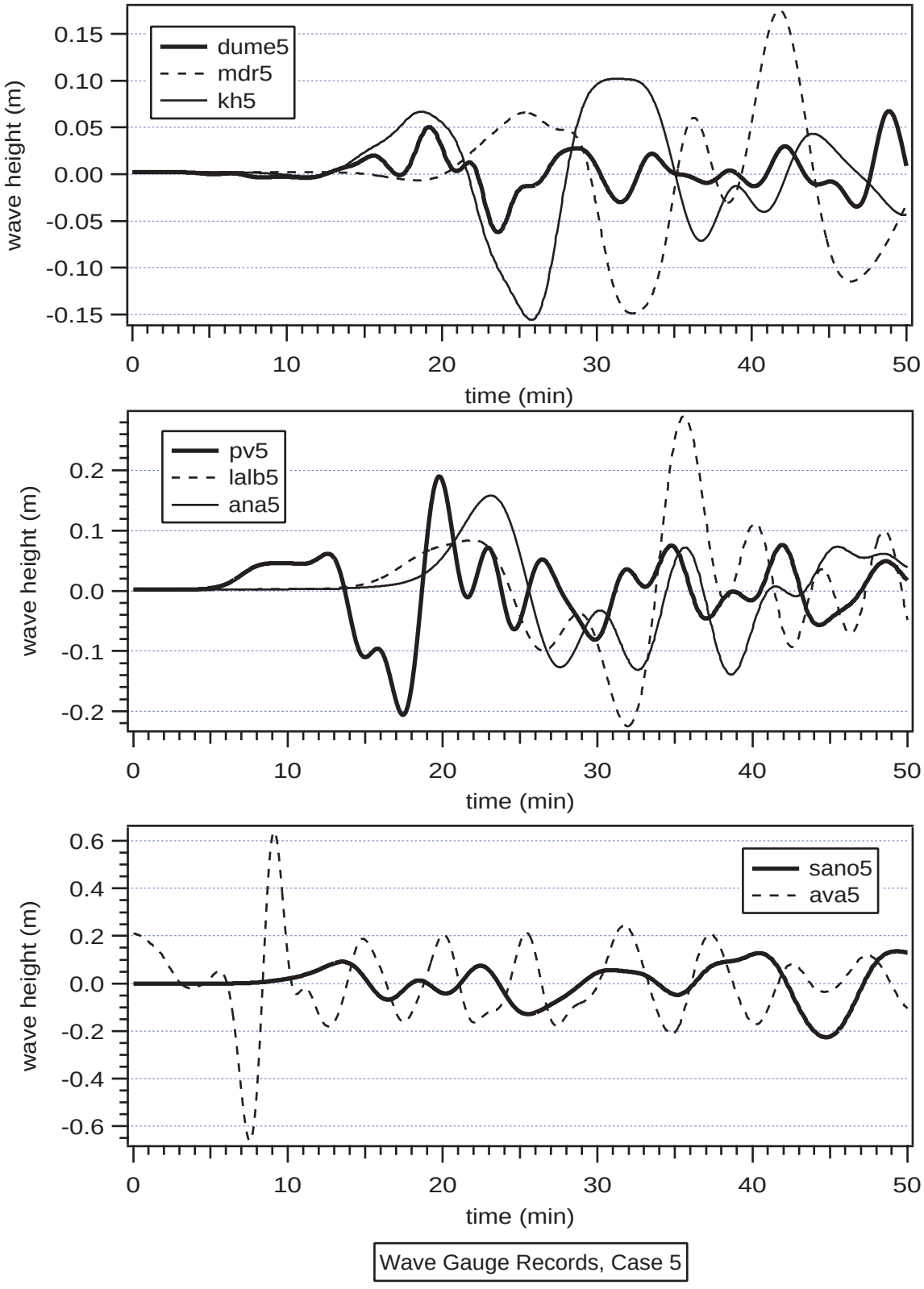

Figure 4. Wave gauge records for segments 2 through 4 of the Catalina fault (M=7.0) earthquake (Case 5).

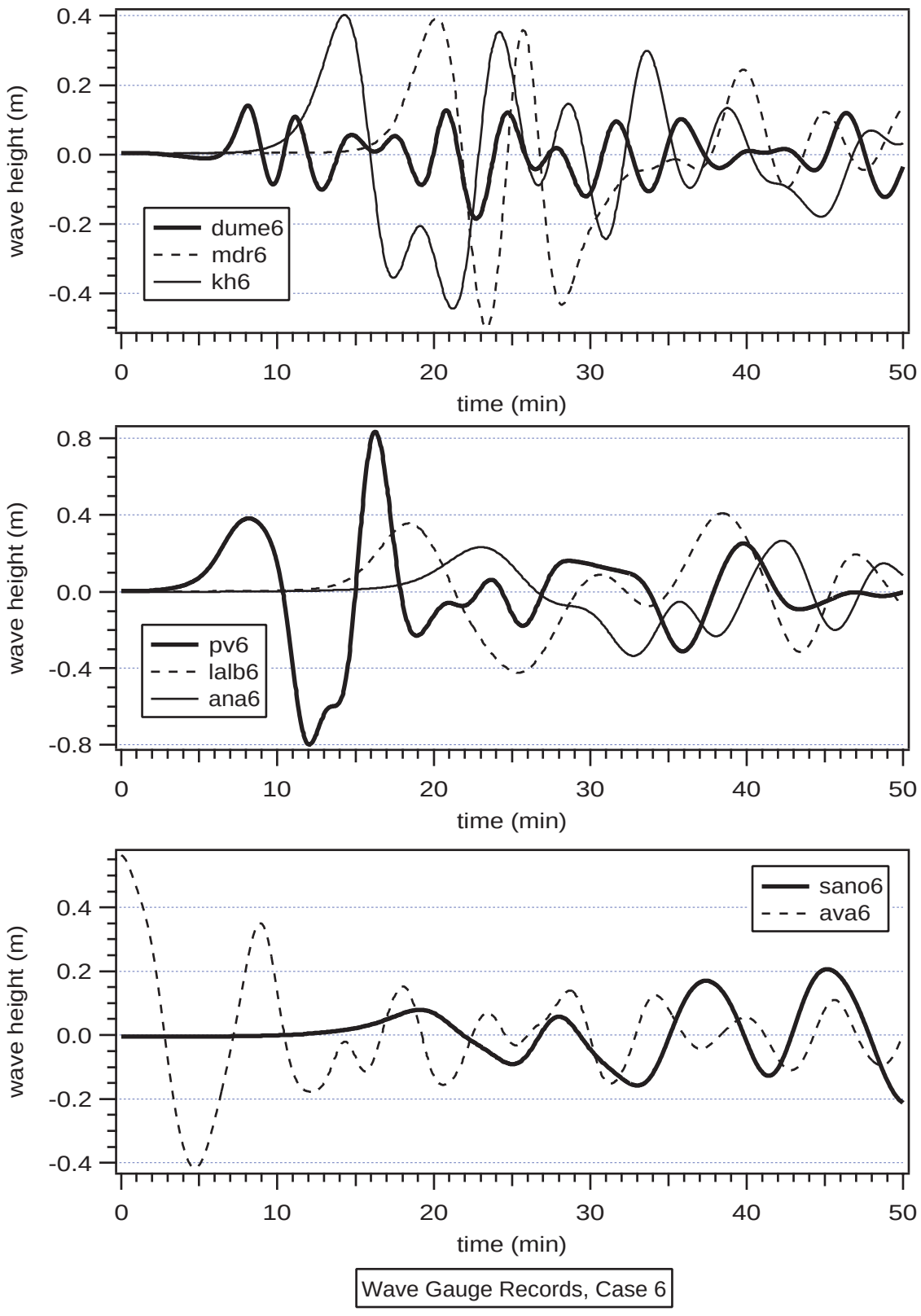

Figure 5. Wave gauge records for segments 5 through 7 of the Catalina fault (M=7.3) earthquake (Case 6).

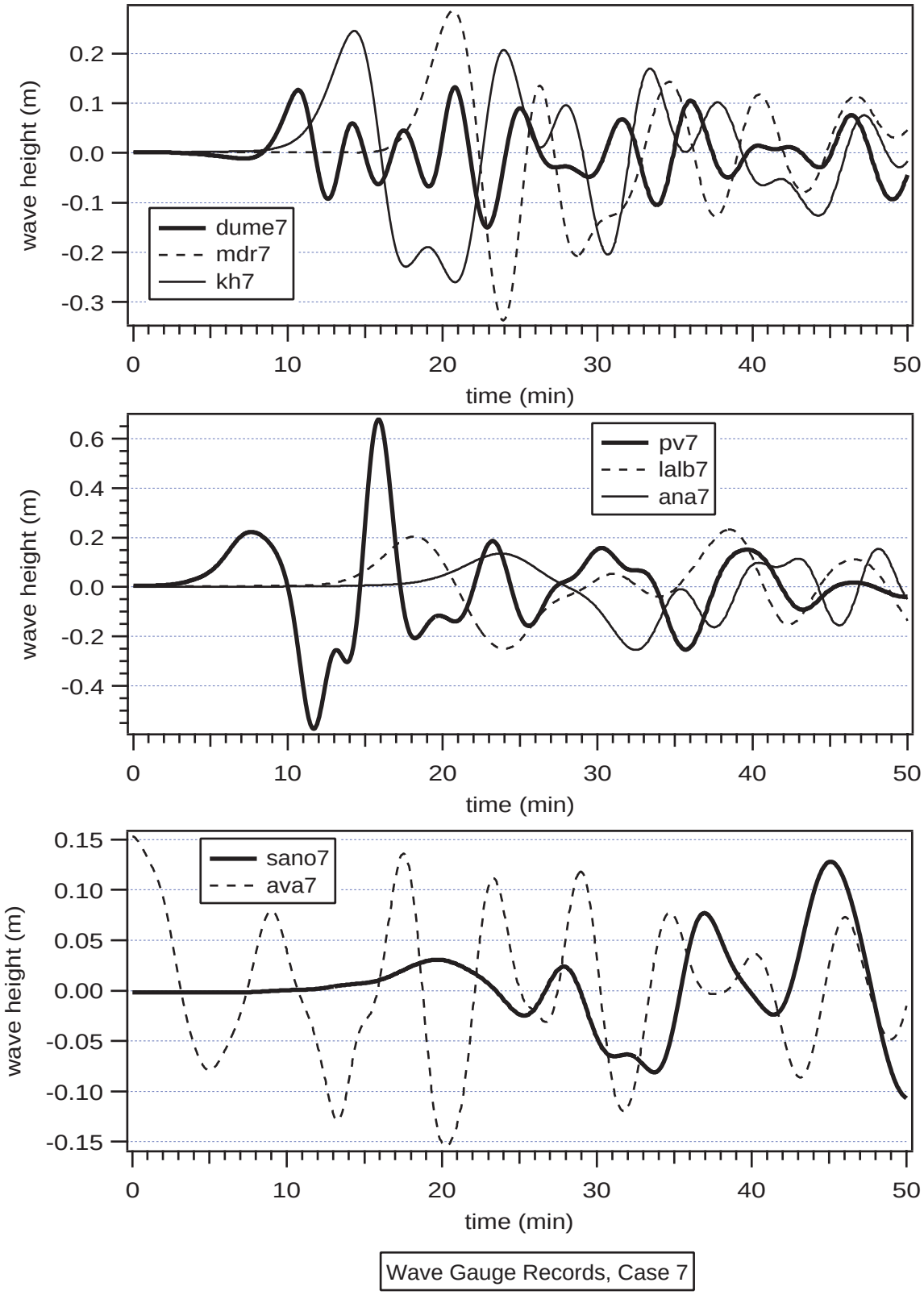

Figure 6. Wave gauge records for segments 5 through 6 of the Catalina fault (M=7.0) earthquake (Case 7).